Circulation: Heart Failure

ORIGINAL ARTICLE

IL1RAP Blockade With a Monoclonal Antibody Reduces Cardiac Inflammation and Preserves Heart Function in Viral and Autoimmune Myocarditis

Diego A. Lema, MD, PhD*; Gabriel Jakobsson, MSc*; Abdel Daoud, MS; David Elias, PhD; Monica V. Talor, MSc; Sara Rattik, PhD; Caitríona Grönberg, PhD; Hannah Kalinoski, PhD; Elin Jaensson Gyllenbäck, PhD; Nadan Wang, MSc; David Liberg, PhD; Alexandru Schiopu, MD, PhD*; Daniela Čiháková, MD, PhD*

BACKGROUND: Currently, there are no therapies targeting specific pathogenic pathways in myocarditis. IL (interleukin)-1 blockade has shown promise in preclinical studies and case reports. We hypothesized that blockade of IL1RAP (IL-1 receptor accessory protein), a shared subunit of the IL-1, IL-33, and IL-36 receptors, could be more efficient than IL-1 blockade alone.

METHODS: We induced coxsackievirus B3 (CVB3)–mediated or experimental autoimmune myocarditis (EAM) in BALB/c mice, followed by treatment with an Fc (fragment crystallizable)-modified mIgG2a mouse anti-mouse IL1RAP monoclonal antibody (mCAN10). Myocarditis severity and immune infiltration were assessed by histology and flow cytometry. Cardiac function was measured by echocardiography. We used spatial transcriptomics (Visium 10× Genomics) to compare the gene expression landscape in the hearts of mCAN10-treated versus control mice.

RESULTS: IL1RAP blockade reduced CVB3 and EAM severity. In EAM, the treatment prevented deterioration of cardiac function, measured on day 42 post-disease induction (left ventricular ejection fraction: 56.5% versus 51.0% in isotype controls [P=0.002] and versus 51.4% in mice treated with anti-IL-1β antibodies alone [P=0.003]; n=10–11 mice per group). In the CVB3 model, mCAN10 did not impede viral clearance from the heart and significantly lowered the numbers of $CD4^+$ (cluster of differentiation 4) T cells (P=0.025), inflammatory $Ly6C^+CCR2^+$ (lymphocyte antigen 6 complex, locus C/C-C motif chemokine receptor 2) monocytes (P=0.038), neutrophils (P=0.001) and eosinophils (P<0.001) infiltrating the myocardium. The spatial transcriptomic analysis revealed reduced canonical IL-1 signaling and chemokine expression in cardiac immune foci in CVB3-infected mice treated with IL1RAP blockade.

CONCLUSIONS: Blocking IL1RAP reduces acute CVB3 myocarditis and EAM severity and preserves cardiac function in EAM. We conclude that IL1RAP blockade is a potential therapeutic strategy in viral and autoimmune myocarditis.

Key Words: eosinophils ■ flow cytometry ■ monocytes ■ myocarditis ■ therapeutics

See Editorial by Toldo et al

Myocarditis is an inflammatory disease of the myocardium affecting 22 of 100 000 people globally, although its prevalence is suspected to be significantly underestimated.[1] The main cause of myocarditis is viral, including adenoviruses and cardiotropic enteroviruses, such as coxsackievirus B3 (CVB3).[2]

Correspondence to: Daniela Čiháková, MD, PhD, Johns Hopkins University, 720 Rutland Ave, Ross 659, Baltimore, MD 21205. Email cihakova@jhmi.edu
*D.A. Lema, G. Jakobsson, A. Schiopu, and D. Čiháková contributed equally.
Supplemental Material is available at https://www.ahajournals.org/doi/suppl/10.1161/CIRCHEARTFAILURE.124.011729.
For Sources of Funding and Disclosures, see page XXX.

Circulation: Heart Failure is available at www.ahajournals.org/journal/circheartfailure

WHAT IS NEW?

- IL1RAP (interleukin-1 receptor accessory protein) is a common subunit of the receptors for the pro-inflammatory cytokines IL (interleukin)-1β, IL-1α, IL-33, and IL-36, which have been implicated in the pathogenesis of myocarditis.
- IL1RAP blockade reduced cardiac inflammation and disease severity in viral myocarditis and protected against cardiac dysfunction in autoimmune myocarditis, with higher efficacy compared with anti-IL-1 treatment alone.

WHAT ARE THE CLINICAL IMPLICATIONS?

- Treating myocarditis to prevent myocardial damage and the subsequent heart failure may require broad anti-inflammatory strategies.
- Targeting IL1RAP during myocarditis is a promising potential therapy against acute inflammatory damage and declining cardiac function.

Nonstandard Abbreviations and Acronyms

αMyHC	α-myosin heavy-chain peptide
CAR	coxsackievirus and adenovirus receptor
CVB3	coxsackievirus B3
d.p.i.	days post-infection
EAM	experimental autoimmune myocarditis
EF	ejection fraction
H&E	hematoxylin and eosin
IFN	interferon
IL	interleukin
IL1R1	interleukin-1 receptor, type 1
IL1Ra	interleukin-1 receptor antagonist
IL1RAP	interleukin-1 receptor accessory protein
ILC2	innate lymphoid cell, type 2
NFκB	nuclear factor-κB
scRNA-Seq	single-cell RNA sequencing
SPADE	Spatial Deconvolution for Domain Specific Cell-Type Estimation
TNF	tumor necrosis factor

Recent studies have indicated that adenovirus is more prevalent as a cause of myocarditis in the United States, based on its frequency in endomyocardial biopsies, compared with enteroviruses. While adenovirus accounts for 23% of cases, enteroviruses remain significant at 14%.[2] Both adenoviruses and enteroviruses are cytolytic viruses that directly target cardiomyocytes by binding to CAR (coxsackievirus and adenovirus receptor), resulting in substantial direct cardiac injury followed by a robust inflammatory response. Myocarditis can also be caused by autoimmune reactions against the heart. Some forms of autoimmune myocarditis such as giant-cell myocarditis have especially poor prognosis, half of these patients requiring heart transplantation within 5 years.[3] Therapies for myocarditis currently focus on supportive care, with some patients requiring mechanical support or transplantation. This can occur in up to 40% of children diagnosed with acute myocarditis.[4] There is an unmet need for therapies targeting the pathogenic mechanisms that drive the disease.

IL1RAP (interleukin-1 receptor accessory protein; also called IL1R3) is a shared subunit for the IL (interleukin)-1, IL-33 and IL-36 isoform receptors. After engaging their cognate cytokines, these receptors form a signaling complex with IL1RAP and activate the MyD88 (myeloid differentiation factor 88)-p38-NFκB (nuclear factor-κB) pathway.[5] Monoclonal antibodies blocking IL1RAP have shown promise in murine models of inflammatory disease including monosodium urate peritonitis, allergic airway inflammation, and psoriasis.[6] The importance of the IL1RAP-dependent cytokines in cardiovascular disease is becoming increasingly evident in recent clinical trials and animal studies. IL-1β is the best-characterized cytokine of this family. The CANTOS trial (Cantos Canakinumab Anti-Inflammatory Thrombosis Outcomes Study) demonstrated that canakinumab, an antibody that neutralizes IL-1β, reduces the recurrence of cardiovascular events in patients with previous myocardial infarction.[7] The magnitude of this effect directly correlated to the reduction of elevated inflammatory markers.[8] The role of IL-33 in cardiovascular disease is less well established.[9] We and others have demonstrated that IL-33 promotes eosinophilic pericarditis and myocarditis.[10] This effect is largely due to the activation of resident cardiac innate lymphoid cells, type 2 (ILC2).[11,12] IL-36 is the least characterized of these cytokines in cardiovascular disease but has been reported to exacerbate endothelial dysfunction, ischemia/reperfusion injury,[13,14] and viral myocarditis[15] in rodent models.

Murine models of myocarditis, particularly CVB3 myocarditis and experimental autoimmune myocarditis (EAM), have provided invaluable clues of the immunopathogenesis of this disease and are important tools for preclinical testing of novel therapies before they advance to human trials.[16,17] Preclinical studies have demonstrated that blocking individual components of the IL-1 signaling pathway[18–20] or neutralizing IL-33 by a soluble decoy receptor[10] may hold therapeutic promise in treating myocarditis. Additionally, indirect promotion of IL-36 signaling through IL-38 blockade exacerbates CVB3 myocarditis, suggesting a potential therapeutic role for IL-36 blockade.[15] We hypothesized that blockade of IL1RAP might be an efficient therapeutic approach in myocarditis, due to simultaneous inhibition of IL-1, IL-33,

and IL-36 signaling.[21] An Fc (fragment crystallizable)-modified hIgG1 humanized anti-human IL1RAP monoclonal antibody (CAN10; Cantargia AB, Lund, Sweden) is under development for treatment of inflammatory and fibrotic diseases and is currently undergoing a phase 1 clinical trial in healthy subjects and in subjects with plaque psoriasis (https://www.clinicaltrials.gov; unique identifier: NCT06143371). In our current study, we evaluated the efficacy of a murine functional equivalent of CAN10 (Fc-modified mIgG2a mouse anti-mouse IL1RAP monoclonal antibody [mCAN10]) for the treatment of viral and autoimmune myocarditis. Our results indicate that mCAN10 has a potent anti-inflammatory profile in myocarditis, reduces disease severity, and prevents deterioration of cardiac function. These findings underscore the potential translational benefit of IL1RAP blockade to treat cardiac inflammatory disease.

METHODS

Data Availability

The Visium spatial transcriptomics data reported in this article have been deposited in Figshare and are accessible with the following link: https://figshare.com/s/165ca561bcf11686d4fe. The remaining data that support the findings of this study are available from the corresponding author upon reasonable request.

Animals

Wild-type BALB/cJ (JAX 651) mice were purchased from The Jackson Laboratories (Bar Harbor, ME). We used 6- to 10-week-old BALB/cJ male mice. Animals were housed at the pathogen-free animal facilities of Johns Hopkins University School of Medicine, Lund University, or at the CL laboratory LCC (Baltimore, MD). Animals were housed under standard conditions with 12-hour light and dark cycles and access to water and food ad libitum. All experiments were performed with age-matched mice in accordance with the guidelines set forth in the Guide for the Care and Use of Laboratory Animals. All methods and protocols were approved by the Animal Care and Use Committee of Johns Hopkins University, the Institutional Animals Care and Use Committee conforming to the Guide for the Care and Use of Laboratory Animals published by the US National Institutes of Health, or by the Regional Ethics Committee for animal research in Lund, Sweden.

Pharmacokinetic Measurements of mCAN10 in Mice

The optimal pharmacokinetic profile of mCAN10 was determined by utilizing healthy female C57BL/6 mice (8 weeks of age) receiving intraperitoneal injections twice weekly for a total of 3 injections, 10 mg/kg per dose with a double dose at the first dosing occasion. Blood was sampled from the sublingual vein, and each mouse was sampled 3×.

A dose-finding study in mice with EAM, induced as described below, was performed in male BALB/c mice (8 weeks old) with dosing starting at day 7 after disease induction. The mice were divided into the following dose groups: 0, 3, 10, 30, and 60 mg/kg, receiving intraperitoneal injections twice weekly of mCAN10, without an initial double dose, for 5 weeks. Blood sampling was performed through retro-orbital bleeding on day 28, and echocardiography was performed to assess left ventricular ejection fraction (EF).

Free mCAN10, not bound to soluble or membrane-bound mouse IL1RAP, was measured in plasma. Mouse plasma was diluted 1:100 and 1:1000. Mouse sIL1RAP (1 µg/mL) was coated on microtiter plates, and free mCAN10 in samples and standards was allowed to bind to the murine sIL1RAP. A biotin-labeled rat anti-mouse IgG2a secondary antibody (MA5-16788; Thermo Scientific) was added and subsequently detected using streptavidin-horseradish peroxidase (N100; Thermo Scientific) and TMB substrate (5120-0047; SeraCare). The resulting absorbance was proportional to the amount of mCAN10 bound on the plate (assay developed by Cantargia AB, Lund, Sweden at Truly Labs AB, Lund, Sweden). Pharmacokinetic analysis was performed through noncompartmental analysis, spares sampling, by using Phoenix WinNonline 8 (Certara).

mCAN10 In Vitro Cytokine Inhibition Assay

NIH3T3 mouse fibroblast cell line (ATCC; CRL1658) cells were grown in DMEM with GlutaMax (Gibco; 61965-026) supplemented with 10% calf bovine serum (Sigma-Aldrich; 12133C; hereafter called complete media). For detachment, cells were rinsed with 1 mL PBS, and then 1 mL 0.25% trypsin-EDTA solution was added to the flask followed by 1-minute incubation at 5% CO_2, 37 °C. The trypsin was neutralized with 10× volume of complete media; cells were washed and seeded in a 96-well plate at a density of 40×10^3 cells per well in 50 µL complete media. Where indicated, cells were blocked with mCAN10 at 20 µg/mL (IL-1β, IL-33, and IL-36) or 60 µg/mL (IL-1α) for 1 hour at 37 °C, 5% CO_2, and then stimulated with recombinant murine IL-1α, IL-1β, IL-33, IL-36α, IL-36β, or IL-36γ (Table) followed by incubation at 37 °C, 5% CO_2, overnight (16–18 hours). After centrifugation, the supernatant was harvested by centrifugation at 1000*g* for 10 minutes at 4 °C and stored at −80 °C awaiting analysis.

Table. Cytokines Used in mCAN10 Cytokine Inhibition Studies

Chemical/material	Vendor	Product number	Lot number	Final concentration, ng/mL
rmIL-1α	R&D Systems	400-ML-005	BL0320041	0.005
rmIL-1β	R&D Systems	401-ML-005	BN0720072	0.03
rmIL-33	Peprotech	210-33	511434	15
rmIL-36α	R&D Systems	7059-ML-010	DARO1118111	15
rmIL-36β	R&D Systems	7060-ML-010	DAQS0318021	8
rmIL-36γ	R&D Systems	6996-IL010	DAQQ0319021	15

This table contains a list of recombinant murine cytokines, where they were sourced from, and the final concentrations used to stimulate NIH3T3 cells in mCAN10 cytokine inhibition studies. rm indicates recombinant mouse.

Luminex xMAP technology was used to quantify G-CSF (granulocyte colony-stimulating factor). The multiplexing analysis was performed using the Luminex 200 system (Luminex, Austin, TX) by Eve Technologies Corporation (Calgary, Alberta) using Eve Technologies' Mouse Cytokine/Chemokine MD31 array according to the manufacturer's protocol.

HEK293 QUANTI-Blue Reporter System

HEK-Blue (IL-1R) cells (originally from Invitrogen) were cultured in complete medium (DMEM+glutamax+10% heat-inactivated calf serum+selection antibiotics). Cells were counted and seeded in 96-well plates (5×10^4 cells per well; 150 µL cell suspension per well) and left for at least 2 hours to attach. The diluted antibodies mCAN10, anti-IL-1β goat IgG2 (AF-401-NA; R&D Systems), or isotype controls were added to the cells and preincubated at 37 °C for 1 hour. After that, IL-1β at a final concentration of 30 pg/mL was added and incubated at 37 °C for 17 hours. Plates were then centrifuged at 300*g* for 5 minutes, 50 µL supernatant was collected and mixed with QUANTI-Blue working solution, followed by incubation for 60 to 90 minutes at 37 °C. Color development was measured at 620 nm using a SpectraMax i3 spectrophotometer (Molecular Device).

CVB3 Myocarditis Induction

Six- to 10-week-old male BALB/cJ mice were infected intraperitoneally with 1.6×10^3 plaque-forming units of BALB/cJ heart-passaged CVB3 (Nancy strain, from Prof Karin Klingel) diluted in 100 µL sterile PBS (PAA Laboratories).

Experimental Autoimmune Myocarditis

EAM was induced by double immunization with a myocardial-specific myosin peptide emulsified in complete Freund adjuvant, as previously described by Fontes et al.[22] In this model, complete Freund adjuvant induces an IL-6–dependent expansion of dendritic cells and monocytes in lymph nodes, spleen, and heart, promoting the generation of autoreactive myosin-specific T cells that induce cardiomyocyte damage. αMyHC (α-myosin heavy-chain peptide; Ac-RSLKLMATLFSTYASADR-OH; AnaSpec) was dissolved in 1 mL PBS to a concentration of 1 mg/mL and emulsified 1:1 in complete Freund adjuvant (Sigma-Aldrich) containing 1 mg/mL *Mycobacterium tuberculosis* (H37Ra). On days 0 and 7, 200 µL emulsion containing 100 µg peptide was injected subcutaneously, divided over the flank and shoulder blade to minimize discomfort from local inflammation. In this model, myocardial inflammation starts on day 7, at the time of the booster immunization, and reaches peak on day 21. This pathogen-free model has been used to assess treatment effects on long-term cardiac function, as it avoids the caveat of virus-induced mortality of the sickest animals encountered in the CVB3 model, which in turn may lead to bias due to falsely higher LV function of the surviving mice.

Antibody and Control Treatments

CVB3-infected mice were treated starting at day 0, and the EAM mice were treated from day 7, at the time of the booster αMyHC immunization. mCAN10 (a monoclonal mouse mIgG2a anti-mouse IL1RAP antibody with L234A, L235A, and P329G [LALA-PG] mutations leading to decreased Fc/FcγR [Fc-gamma receptor] effector functions) and isotype control (anti-HEL mIgG2a-LALA-PG) were administered intraperitoneally as a loading dose of 20 mg/kg on the first injection, followed by biweekly injections of 10 mg/kg. The dose of mCAN10 was selected based on the mouse pharmacokinetics study and the dose range finding study described above. Treatment with 10 mg/kg twice a week with an initial loading dose of 20 mg/kg saturates sIL1RAP, gives stable mCAN10 levels in plasma, and has the best effect on heart function deterioration (Figure S1). Animals receiving αIL-1β (goat IgG2, AF-401-NA; R&D Systems) or isotype control goat-IgG2 were given biweekly injections of 0.5 mg/kg. The dose of anti-IL-1β was chosen based on a previous publication.[23] This anti-IL-1β antibody is highly potent and inhibits IL-1β signaling in the HEK293 QUANTI-Blue reporter system at an 80× higher potency compared with mCAN10 (Figure S1J). In selected in vivo experiments, we compared the efficacy of mCAN10 with prednisone or with the IL1Ra (IL-1 receptor antagonist), anakinra. Prednisone was administered p.o. daily at 5 mg/kg, and IL1Ra was given s.c. daily at 25 mg/kg. These treatment regimens were selected based on available literature showing effects with the indicated doses. The IL1Ra dose was chosen to be as close as possible to the clinical human dose, and daily s.c. injections were used because of the short half-life of the drug.[24,25] In a separate EAM study performed by CL Laboratory LLC (Gaithersburg, MD), treatment with mCAN10 or isotype control was initiated on day 14 to assess the effects of the antibody on already established myocarditis.

Viral Titer Determination With the Plaque Assay

Vero cell lines were plated in 24-well plates, grown to 90% confluency, and infected with 55 µL of samples containing virus. After a 60-minute incubation at 37 °C, warm methylcellulose solution was added and solidified within the wells for 3 days, followed by adding 10% phosphate-buffered formalin fixative solution. Solutions in the wells were aspirated, and 1% (w/v) crystal violet dye was added to visualize the plaques. The plates were rinsed with running water, and the number of plaques per well was counted and converted to the viral titer (plaque-forming units/mL).

Flow Cytometry and Single-Cell Preparations

Flow cytometry samples from CVB3 tissues were prepared in a BSL2 hood. Mouse hearts were flushed in situ with PBS for 2 minutes, harvested, digested, and filtered into single-cell suspensions using mechanical disruption with a GentleMACS Dissociator (Miltenyi), enzymatic digestion (collagenase II and DNase I, Worthington), and 40-µm cell strainers (Falcon) as described previously.[11] Spleens were dissociated into single cells with 40-µm cell strainers, and red blood cells were lysed with ACK (ammonium chloride lysine buffer) solution (Quality Biological). Bone marrow was flushed from the right femur with DMEM using a 25G needle and 3-mL syringe, and the resulting cells were strained and red blood cells lysed.

For flow cytometry, cardiac and splenic single cells were first stained with Live/Dead Aqua Fixable Dye (Invitrogen). After FcRγII/III block with TruStain FcX anti-mouse CD16/32 (cluster of differentiation 16/32; BioLegend), cells were surface stained in the fluorescence-activated cell sorting buffer (0.5% BSA, 2 mmol/L EDTA in PBS) with a cocktail of

fluorochrome-conjugated antibodies against CCR2 (C-C motif chemokine receptor 2; SA2036-11, BV421), Ly6G (lymphocyte antigen 6 complex, locus G; 1A8; Pacific Blue), CD44 (1M7, BV480), CD206 (CO68C2, BV605), CD8 (53-6.7, BV650), CD64 (X54-517-1, BV711), CD90 (30-H12, BV750), Ly6C (HK1.4, BV785), CD3 (145-2C11, FITC [fluorescein]), KLRG1 (killer cell lectin-like receptor G1; 2F1, Alexa Fluor 532), NKp46 (29A1.4, PerCP [peridinin-chlorophyll-protein]-Cy5.5), ST2 (soluble interleukin 1 receptor-like 1 cardiac biomarker; RMST2-33, PerCP-eFluor 710), Siglec F (E50-2440, PE [phycoerythrin]), CD45 (HI30, PE-Texas Red), CD62L (MEL-14, PE-Cy5), F4/80 (BMP [B-type natriuretic peptide], PE-Cy7), MerTK (mer proto-oncogene tyrosine kinase; 2B10642, APC [allophycocyanin]), IL1RAP (15F12, Alexa Fluor 647), CD4 (GK1.5, Alexa Fluor 647), MHC-II (major histocompatibility complex class II; M5/114.15.2, Alexa Fluor 700), and CD11b (M1/70, APC-eFire750). Bone marrow cells were stained with LIVE/DEAD Aqua, followed by staining with a CD16/32 antibody (S17011E, APC-Cy7), before proceeding to FcRγII/III block as described above. The cells were stained with a mix of antibodies against CD135 (A2F10, BV421), Sca-1 (spinocerebellar ataxia type 1; D7, BV605), CD150 (TC15-12F122, BV711), a lineage (CD3, CD11b, CD19, B220, Ter-119, Ly6C, Ly6G), cocktail (145-2C11; RB6-8C5; RA3-6B2; Ter-119; M1/70, FITC), CD34 (RAM34, Alexa Fluor 532), IL7R (A7R34, PE), CD45 (HI30, PE-Texas Red), c-Kit (ACK2 [antibody that binds to CD117], APC), and CD48 (HM48-1, Alexa Fluor 700). All antibodies were purchased from BD Biosciences, BioLegend, eBioscience, Miltenyi, or R&D Systems, with the exception of IL1RAP, which was purified in-house. Cells were fixed with CytoFix Buffer (BioLegend). Sample acquisition was performed on a 4-laser Cytek Aurora spectral flow cytometer (Cytek) running SpectroFlo (Cytek). Data were analyzed using the FlowJo v8.10.0 software (BD Biosciences) and SpectroFlo (Cytek). Gating parameters were defined on the first sample and applied to all samples in the same experiment, minimizing the risk for observer bias. The observer was not blinded to the identity of the groups.

Myocarditis Severity Grading

For the histological and immunohistochemical analyses, hearts were fixed with 10% buffered formalin, embedded in paraffin, and sectioned at 5 µm, as described previously.[26] One middle section per heart was stained with hematoxylin and eosin (H&E). Inflammation levels were assessed in the entire section by grading the area of infiltration with immune cells as follows: grade 0, no inflammation; grade 1, <10% of the heart section is infiltrated; grade 2, 10% to 30%; grade 3, 30% to 50%; grade 4, 50% to 90%; and grade 5, >90%. Three blinded, independent observers graded each heart, and their scores were averaged.

Fibrosis Severity Grading

One middle section per heart was stained with Masson trichrome. Fibrotic area and whole area were measured using computerized planimetry (Image J; National Institutes of Health). The fibrotic area was presented as a percentage of the whole area. Three random fields per heart were counted and averaged. A total of 30 fields per group were measured in the study. The observer was blinded to the origin of the cardiac sections.

Immunohistochemistry

For CD68 and Ly6G staining, antigen retrieval was performed by boiling the sections in 10-mmol/L citrate buffer at pH 6.0 for 15 minutes, followed by blocking with 10% BSA and incubation with anti-CD68 (Ab125212; Abcam) or anti-Ly6G (551459; BD Pharmingen) overnight. Antibody detection was performed with biotinylated species-specific secondary antibody (goat anti-rabbit BA-1000 or rabbit anti-rat BA-4001, respectively; Vector Laboratories), followed by streptavidin-conjugated horseradish peroxidase (VECTASTAIN Elite ABC; Vector Laboratories) and developed with the DAB ImmPACT kit (SK-4105; Vector Laboratories). Slides were imaged with a ScanScope GL (Aperio). Positive staining was quantified using QuPath.

Light Microscopy

Images on H&E-stained, Masson trichrome–stained, and Picrosirius red–stained and immunostained sections were acquired on the BX43 microscope (Olympus) with the DS-Fi3 camera (Nikon) using NIS-Elements D Software (v. 5.10.01; Nikon).

Echocardiography

In the CVB3 myocarditis model, transthoracic echocardiography was performed on conscious mice using the Vevo 3100 imaging system (VisualSonics) with an MX-550D probe. The animals were placed in supine position, shaved with depilatory cream, and prewarmed ultrasound gel was applied to the chest. The animals were maintained at 37 °C during the measurements. Parasternal short-axis M-mode images were collected and left ventricular function was calculated in Vevo LAB (VisualSonics) using the Teichholz method. For the EAM experiments, transthoracic echocardiography was performed on mice under isoflurane inhalatory anesthesia, using the Vevo 3100 imaging system (VisualSonics) with an MX-550D probe. B-mode images were collected in the parasternal long axis in the center of the heart with the apex and the aorta as reference, in accordance with the study by Lindsey et al.[27] The left ventricular function was analyzed in Vevo LAB (VisualSonics) by tracing of the left ventricle outline in systole and diastole. The left ventricular EF was calculated based on the measurement of left ventricular volumes by the Simpson method. In the late-treatment EAM experiments, images were obtained with an Acuson P300 (Siemens) and a linear array transducer probe. Three to 5 consecutive beats were averaged for all studies. All measurements and analyses were performed by blinded investigators.

Quantitative Real-Time Polymerase Chain Reaction

Total RNA was extracted from tissues using RNeasy Plus Mini Kit (Qiagen). Single-stranded cDNA was synthesized with iScript Reverse Transcription Supermix (BioRad). A CVB3 strain Nancy UTR (complete genome: GenBank JX312061.1) was amplified using the following primers: forward: 5′-CCC TGA ATG CGG CTA ATC C-3′ and reverse: 5′-ATT GTC ACC AA AGC AGC CA-3′. Power SYBR Green PCR Master Mix (Applied Biosystems) was used, and real-time cycle thresholds were detected via MyiQ2 thermal cycler (BioRad). Data were analyzed by the $2^{-\Delta\Delta Ct}$ method and were normalized to *Gapdh* expression and then to biological controls.

Serum Cardiac and Inflammatory Biomarker Determination

Mice were bled retro-orbitally using heparinized capillary tubes under general anesthesia before euthanization, and serum was separated by centrifugation. Mouse high-sensitivity T-cell magnetic bead panel from Millipore Sigma (MHSTCMAG-70K) was used to measure the levels of cytokines in the serum. This kit measures 18 different mouse cytokines (GM-CSF [granulocyte-macrophage colony-stimulating factor], IFN [interferon]-γ, IL-1α, IL-1β, IL-2, IL-4, IL-5, IL-6, IL-7, IL-10, IL-12 [p70], IL-13, IL-17A, KC [murine embryonic fibroblasts], LIX [lipopolysaccharide-induced], MCP-1 [monocyte chemoattractant protein-1], MIP-2 [macrophage inflammatory protein-2], and TNF [tumor necrosis factor]).

Single-Cell RNA-Sequencing Analysis

A publicly available single-cell RNA-Seq cardiac data set (Gene Expression Omnibus accession code: GSE174458) representing 2 healthy mouse hearts and 2 CVB3-infected myocarditis mouse hearts, a publicly available single-cell RNA sequencing (scRNA-Seq) healthy bone marrow data set (Gene Expression Omnibus accession code: GSE75478) representing 2 healthy donors, and a publicly available healthy heart scRNA-Seq data set (Extractable Nuclear Antigen accession number: ERP123138) representing 14 healthy donors were analyzed for the expression of IL1RAP (and IL1R1 [IL-1 receptor, type 1] where applicable). For each data set, The SCTransform Seurat pipeline, using a Seurat (v4.1.1) package, was utilized for scRNA-Seq processing and clustering. Canonical phenotype markers verified using the FindAllMarkers() function were used to identify cell populations. Feature plots were generated using the FeaturePlot() function, and dot plots were generated using the DotPlot() function. Each data set was analyzed separately. All scRNA-Seq analyses and visualization were performed with R (v4.1.1).

Spatial Transcriptomics

Spatial transcriptomics was performed by the Johns Hopkins Single Cell and Transcriptomics Core using the Visium platform (10× Genomics). Mouse hearts were formalin fixed, paraffin embedded, H&E stained, and imaged as described above. Hard set coverslips were removed by submerging in xylene and placing in a precooled metal block. Then, slides were destained in xylene followed by decreasing concentrations of ethanol solutions. A small piece of tissue from a different heart section on the same slides was scraped off to assess RNA integrity by DV200 determination. CytAssist (10× Genomics) was used to facilitate transfer of heart sections to the capture area of the Visium slides (11×11 mm). Sequencing was performed according to the manufacturer's instructions. Spatial transcriptomic libraries were generated using the Visium Spatial Gene Expression Reagent Kit (10× Genomics). Raw sequencing data were preprocessed and demultiplexed using Space Ranger (v1.2.0; 10× Genomics). Consequently, reads were analyzed according to the Seurat (v 4.1.1) spatial workflow. Further statistical analysis was strictly conducted on either immune foci or fibroblast spots. Immune foci spots were defined as spots with a normalized *Ptprc* (CD45) expression >0. Fibroblast spots were defined as spots with a normalized *Ptprc* (CD45) expression =0 and a normalized *Pdgfra* expression >0. Statistical analysis of genes spatially variable between spatial transcriptomic slides was conducted using the Spatial Deconvolution for Domain Specific Cell-Type Estimation (SPADE) package (v1.0). Following the SPADE analysis, $\log_2$(fold change) between mCAN10-treated and isotype-treated immune foci or fibroblast areas was examined. Only genes with an adjusted $P \leq 0.05$ and $\log_2$(fold change) <0 were retained. Visualization involving histological slides was conducted in python using the scanpy package (v 5.2.1). The use of the standardized pipeline and the SPADE analysis described above reduces the risk of bias to a minimum. The observer was not blinded to the identity of the groups.

Statistics

GraphPad Prism 8 was used for statistical analysis. Comparisons between 2 groups were analyzed using the Student *t* test. Comparisons between ≥3 groups were performed with 1-way ANOVA or Kruskal-Wallis test with Dunn pairwise multiple post hoc comparisons. For repeated measures experiments, a 2-way ANOVA with Fisher least significant difference multiple comparisons post hoc test was used. Data are represented as mean±SD for normally distributed values or as median for non-normally distributed data. Statistically significant *P* values are presented in the figures and text.

RESULTS

IL1RAP Is Expressed in Mouse Hearts and Bone Marrow

We used flow cytometry to investigate the expression of IL1RAP in immune and nonimmune populations of the heart and bone marrow in naive or CVB3-infected mice euthanized on day 10 post-infection. In the heart, IL1RAP was highly expressed in $CD64^+F4/80^+$ monocytes/macrophages, fibroblasts, and eosinophils (Figure 1A). Neutrophils and cardiac ILC2s, a population that is dependent on IL-33 stimulation,[11,12] also expressed IL1RAP. All T-cell subsets showed low expression of IL1RAP (mean fluorescence intensity [MFI], <5000). IL1RAP expression increased in $CD4^+$ T central memory cells ($CD4^+$ Tcm), naive CD4 T cells ($CD4^+$ Tn), and naive CD8 T cells ($CD8^+$ Tn) during CVB3 myocarditis (Figure 1A). In the mouse bone marrow, IL1RAP expression was the lowest in common lymphoid progenitors (MFI 4676) and multipotent progenitors (MFI 5086) and the highest in $Lineage^{neg}Sca\text{-}1^-c\text{-}Kit^+$ progenitors (MFI 9461) and granulocyte-monocyte precursors (MFI 10375; Figure 1B and 1C).

We sought to corroborate these findings at the gene expression level by using a publicly available sequencing data set of single cells from naive and CVB3-infected mice at day 21 post-infection.[28] In the naive heart, stromal cells such as smooth muscle cells and fibroblasts expressed high levels of the IL-1 receptor (*Il1r1*) and *Il1rap* (Figure 1D). During CVB3 myocarditis, *Il1rap*

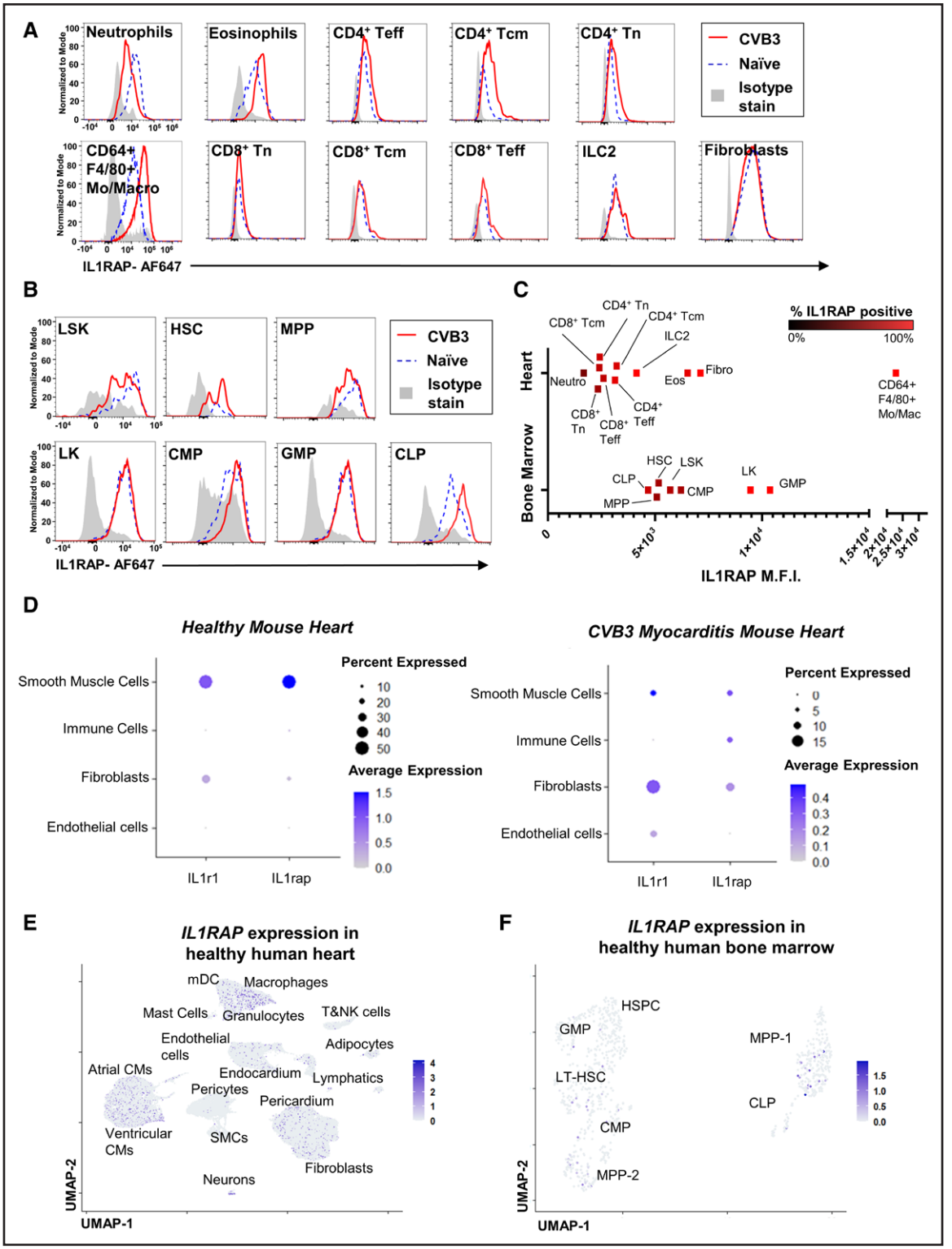

Figure 1. IL1RAP (interleukin-1 receptor accessory protein) expression in the heart and bone marrow during acute viral myocarditis.

A, Histograms of IL1RAP expression levels on immune cell subsets in naive or coxsackievirus B3 (CVB3)–infected (day 10) mouse hearts as assessed by flow cytometry. Cells were stained with anti-IL1RAP-Alexa Fluor 647 or isotype control to establish fluorescence baseline. The *x* axis is the fluorescence intensity of the anti-IL1RAP Alexa Fluor 647 signal. The *y* axis is the cell counts normalized to mode. **B**, Flow cytometry histograms indicating the expression of IL1RAP in bone marrow populations during naive state and CVB3 myocarditis (day 10). **C**, IL1RAP MFI (baseline isotype fluorescence subtracted) for each of the indicated heart and bone marrow populations during acute CVB3 myocarditis (day 10). Frequency of IL1RAP$^+$ cells within each population is indicated by the color of the points. **D**, Dot plots showing the naive and CVB3 myocarditis expression of *Il1r1* (encoding IL1R1) and *Il1rap* (encoding IL1RAP) in various cardiac cell populations utilizing a (*Continued*)

expression was similar in immune cells, fibroblasts, and smooth muscle cells (Figure 1D).

To examine whether IL1RAP is also expressed in human cells, we obtained publicly available scRNA-Seq data sets from the healthy human heart[29] and bone marrow[30] samples. In healthy human hearts, *IL1RAP* is predominantly expressed in macrophages and granulocytes. Other immune populations, such as T cells, showed low expression. *IL1RAP* was also expressed in nonimmune cells, including atrial and ventricular cardiomyocytes, fibroblasts, and endothelial cells (Figure 1E). *IL1RAP* expression in the human bone marrow was sparse and limited to a few populations of multipotent progenitors (Figure 1F).

IL1RAP Blockade by mCAN10 Reduces Acute Myocarditis Severity in CVB3 Myocarditis

We next utilized the mouse anti-mouse IL1RAP monoclonal antibody mCAN10 to block IL1RAP-mediated signaling. mCAN10 is a pure blocking antibody as it contains an LALA-PG modification in the Fc region to prevent FcγR-mediated functions such as antibody-dependent cellular cytotoxicity.[31] We confirmed in vitro that mCAN10 is an effective blocker of IL1α, IL-1β, IL-33, IL-36α, IL-36β, and IL-36γ activity (Figure S1A through S1F) and determined the pharmacokinetic profile of mCAN10 in BALB/c mice with myocarditis and in healthy C57BL/6 mice. The optimal dosing regimen was set to 10 mg/kg biweekly intraperitoneally, with a loading dose of 20 mg/kg (Figure S1G through S1I). The higher tested doses of 30 and 60 mg/kg did not offer additional cardioprotection.

To study the effect of IL1RAP blockade in acute myocarditis, we induced CVB3 myocarditis by injecting BALB/cJ male mice with heart-passaged CVB3 followed by mCAN10 treatment on 0, 3, and 8 days post-infection (d.p.i.; Figure 2A). Mice were euthanized on day 10, at the peak of CVB3 myocardial inflammation.[32] We used 3 control treatment groups: isotype (administered at the same dosage and schedule as mCAN10), IL1Ra, which blocks IL-1 signaling without interfering with the IL-33 or IL-36 receptors (25 mg/kg subcutaneously daily), or PBS (n=10 per group).

The mCAN10-treated animals displayed significantly reduced myocarditis severity, as evaluated by histology, compared with the isotype and PBS groups (IL1RAP versus isotype control myocarditis severity score: 1.1±0.49 versus 2.2±0.75; *P*=0.010; Figure 2B and 2C). mCAN10-treated hearts showed a reduced number of inflammatory foci, which were smaller and less dense than their control counterparts. In contrast, the IL1Ra treatment did not significantly affect the myocarditis severity score compared with PBS. To investigate whether the reduction of myocarditis severity was associated with improved heart function, we performed transthoracic M-mode echocardiography. At 9 d.p.i., we found no statistically significant differences between the left ventricular EF and end-systolic volumes in the mCAN10, IL1Ra, isotype control, and PBS groups (Figure 2D through 2F).

All CVB3-infected animals gradually lost weight during the course of the disease, but this was less severe in the mCAN10 group (*P*=0.006) where weight plateaued on day 8 post-infection, suggesting gradual recovery (Figure 2G). There was no difference in the heart and spleen weights corrected to body weight among treatment groups (Figure 2H and 2I). We also assessed viral persistence in the heart by quantitative polymerase chain reaction detection of viral genome in cardiac tissue at 10 d.p.i. At this time point, 30% to 50% of the mice in each group had cleared CVB3 from the heart with no significant differences in CVB3 RNA levels (mCAN10 [3.307] versus isotype [1.860]; *P*=0.480) or clearance among groups (Figure S2A). This suggests that IL1RAP blockade results in reduced CVB3 myocarditis severity without affecting viral clearance at day 10.

Blocking IL1RAP Reduces Inflammatory Monocytes, T Cells, Neutrophils, and Eosinophils in the Heart in Acute CVB3 Myocarditis

We used spectral flow cytometry to phenotypically characterize the changes in cardiac immune cells on the peak of inflammation, at day 10 of CVB3 myocarditis. The gating strategy is presented in Figure S2B. In accordance with our histological observations, mCAN10 potently reduced the numbers of $CD45^+$ immune cells infiltrating the heart (121.3±80.45 cells/mg) compared with its isotype (320.2±111.97 cells/mg) and PBS controls (328.8±131.94 cells/mg; *P*=0.013 and *P*=0.004, respectively; Figure 3A). Several immune populations in the hearts of the mCAN10 group were reduced compared with isotype, particularly the number of $Ly6C^+CCR2^+$ monocytes (*P*=0.038), macrophages ($CD64^+F4/80^+CCR2^-Ly6C^-$; *P*=0.014), neutrophils

Figure 1 Continued. publicly available single-cell RNA sequencing data set (GSE174458). **E** and **F**, UMAP of publicly available single-cell RNA sequencing data sets showing the expression of *IL1RAP* in the healthy human heart (**E**; ERP123138) and bone marrow (**F**; GSE75478) populations. CLP indicates common lymphoid progenitor; CM, cardiomyocyte; CMP, common myeloid progenitor; Eos, eosinophil; Fibro, fibroblast; GMP, granulocyte-monocyte precursor; HSC, hematopoietic stem cell; Lin, lineage; LK, $Lineage^{neg}Sca\text{-}1^-c\text{-}Kit^+$ precursor; LSK, $Lineage^{neg}Sca\text{-}1^+c\text{-}Kit^+$ precursor; mDC, monocyte-derived dendritic cell; MFI, mean fluorescence intensity; Mo/Mac, monocyte/macrophage; MPP, multipotent progenitor; Neutro, neutrophil; SMC, smooth muscle cell; Tcm, T central memory cell; Teff, T effector cell; Tn, T naive cell; and UMAP, uniform manifold analysis and projection.

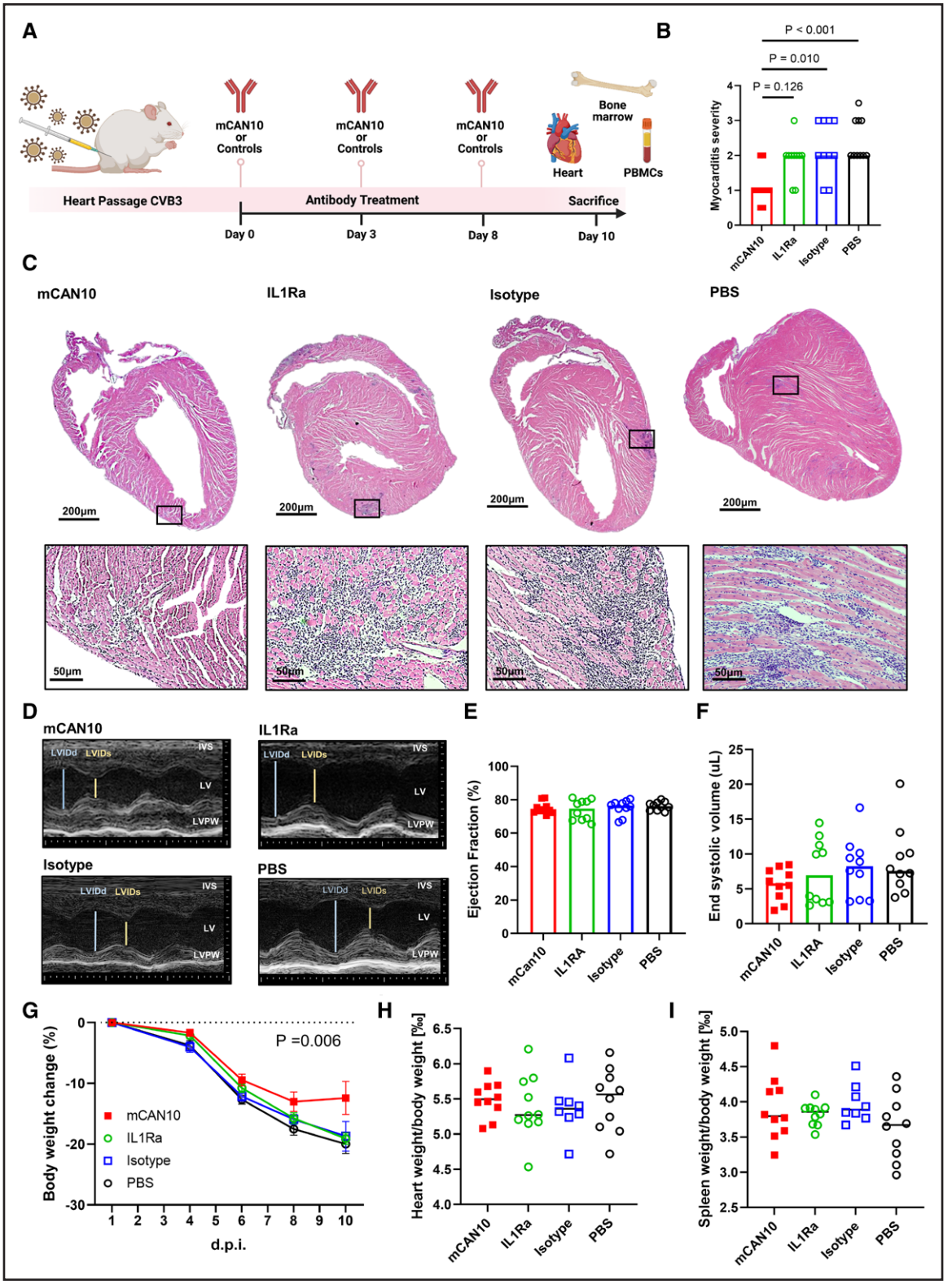

Figure 2. IL1RAP (interleukin-1 receptor accessory protein) blockade by mCAN10 reduces disease severity in acute CVB3 myocarditis.

A, Acute CVB3-myocarditis experimental timeline. All mice were infected with CVB3 virus on day 0 and treated with mCAN10 (n=10), isotype control (n=10), IL1Ra (interleukin-1 receptor antagonist; n=10), or PBS (n=10). Mice were given a loading dose of 20 mg/kg mCAN10 or isotype intraperitoneally on day 0 and were subsequently treated with either of the 2 antibodies at a 10-mg/kg dose biweekly. IL1Ra was administered subcutaneously at 25 mg/kg daily. An equal volume (100 μL) of PBS was administered subcutaneously daily as control. Mice were euthanized on day 10 post-infection. **B**, Myocarditis was scored on H&E–stained sections as described in Methods. Comparison of myocarditis severity score among treatment groups (n=10 mice per group, 3 sections per mouse; Kruskal-Wallis test). (*Continued*)

(P=0.001), and eosinophils (P<0.001; Figure 3B through 3F). We further characterized the immunophenotype of the monocytes and found a minor reduction in MHC-II expression in the Ly6C$^+$CCR2$^+$ subset but no changes in the efferocytosis markers MerTK and CD206 (Figure S2E through S2J). The T-cell subpopulations were also affected by the treatment. Total CD4$^+$ (P=0.025) but not CD8$^+$ T cells decreased with mCAN10 treatment (Figure 3G and 3H). IL1Ra lowered the number of cardiac neutrophils to the same levels as mCAN10; however, this effect did not reach statistical significance compared with the PBS control group (Figure 3D). In summary, mCAN10 reduced cardiac immune cell infiltration more broadly compared with IL-1 blockade alone in the CVB3 myocarditis model at 10 d.p.i.

mCAN10 Reduces Abnormal Bone Marrow Leukocyte Production During Acute CVB3 Myocarditis

During cardiovascular disease, inflammatory mediators produced in the heart and vessel walls, including IL-1β, stimulate leukocyte production in the bone marrow followed by recruitment to sites of inflammation. This establishes a pathological feed-forward loop that contributes to disease progression.[33] To investigate whether IL1RAP blockade could blunt the increased generation of inflammatory cells in the bone marrow during CVB3 myocarditis, we performed flow cytometry analysis of femur bone marrow at 10 d.p.i. (n=10 per group). The gating strategy is presented in Figure 4A and Figure S3A. Compared with PBS-treated animals, the mice receiving mCAN10 displayed significantly reduced numbers of several bone marrow progenitors, including global numbers (Lineage^{neg}CD45$^+$), Lineage^{neg}Sca-1$^+$c-Kit$^+$ progenitors, and its hematopoietic stem cell subset (CD135$^-$CD150$^-$ hematopoietic stem cell). We also observed less Sca-1$^-$c-Kit$^+$ progenitors, in both their IL7R$^+$ lymphoid (common lymphoid progenitors) and myeloid differentiation paths. Common myeloid progenitors (CD16/32$^-$CD34$^+$) and granulocyte-monocyte precursors (CD16/32$^+$CD34$^+$) were reduced by the treatment (Figure 4B through 4J). The numbers of Lineage^{neg}Sca-1$^+$c-Kit$^+$ and hematopoietic stem cell progenitors were significantly lower in mCAN10-treated compared with IL1Ra-treated mice (Figure 4C and 4D). Importantly, treating naive BALB/cJ mice with mCAN10 did not affect the numbers of steady-state bone marrow progenitors (Figure S3B), indicating that mCAN10 only affects the abnormal inflammation-induced hematopoiesis in diseased mice.

We also investigated the effects of mCAN10 on serum cytokines and splenic cell populations (Ly6C$^+$ monocytes, CD4 and CD8 T cells, NK (natural killer) cells, B cells, ILC2, neutrophils, and eosinophils) in mice with CVB3 myocarditis. None of these parameters differed significantly between treatment groups (data not shown).

In conclusion, the mCAN10 treatment does not affect steady-state hematopoiesis but reduces the inflammatory cell population precursors in the bone marrow during acute viral myocarditis.

mCAN10 Reduces the Inflammatory Cardiac Immune Landscape During Viral Myocarditis

To gain a deeper understanding of how mCAN10 treatment affected CVB3 myocarditis at the molecular level, we studied the cardiac immune landscape modifications exerted by IL1RAP blockade, by using the 10× Genomics Visium spatial transcriptomics platform. Archived formalin-fixed, paraffin-embedded, H&E-stained slides from the acute CVB3 myocarditis experiments were used, selecting mice with representative CVB3 myocarditis severity scores and flow cytometry parameters for each treatment.

We performed uniform manifold analysis and projection clustering of spatially localized gene expression spots. This analysis identified a uniform manifold analysis and projection cluster that contained the majority of the spatial spots that expressed *Ptprc* (CD45), *Ccr2*, *Fcgr3* (CD16), and *Lck*, among other canonical gene markers of inflammatory leukocyte populations (Figure S4A). Thus, this cluster was considered to represent the inflammatory foci. This cluster was smaller in mCAN10-treated hearts compared with control treatments (Figure 5A).

Next, we leveraged spatial transcriptomics to visualize the histological areas where immune-related genes and pathways were expressed in the inflamed hearts and compared them across all 4 treatment groups (Figure 5B). *Ccr2* localized primarily to the foci of inflammation and was expressed less and in fewer spots in mCAN10 hearts than in all controls (P<0.001; Figure 5B through 5D), while IL1Ra-treated mice presented an intermediate phenotype. The canonical NFκB pathway was broadly expressed in control treatment hearts

Figure 2 Continued. Data are presented as mean±SD. **C**, Representative H&E-stained heart sections of all treatment groups. **Top**, 1×, scale bar=200 µm; **bottom**: 20×, scale bar=50 µm. **D**, Representative M-mode echocardiography strips. *x* axis: large ticks=0.1 s. *y* axis: ticks=1 mm. **E**, Left ventricular ejection fraction for each treatment group. Data are presented as mean±SD. **F**, Left ventricular end-systolic volume. Data are presented as mean±SD. **G**, Percent body weight change, intergroup differences analyzed by 2-way ANOVA, the *P* value for interaction between treatment and time is shown on graph. **H** and **I**, Heart weight/body weight and spleen weight/body weight ratios, respectively. **B**, **E**, **F**, **H**, and **I**, Kruskal-Wallis test with Dunn multiple pairwise comparisons. *P* values are presented only where the difference between the groups was significant or where there was a trend. All other intergroup comparisons were nonsignificant. CVB3 indicates coxsackievirus B3; H&E, hematoxylin and eosin; IVS, interventricular septum; LV, left ventricle; LVIDd, left ventricular internal diameter, diastole; LVIDs, left ventricular internal diameter, systole; and LVPW, left ventricular posterior wall.

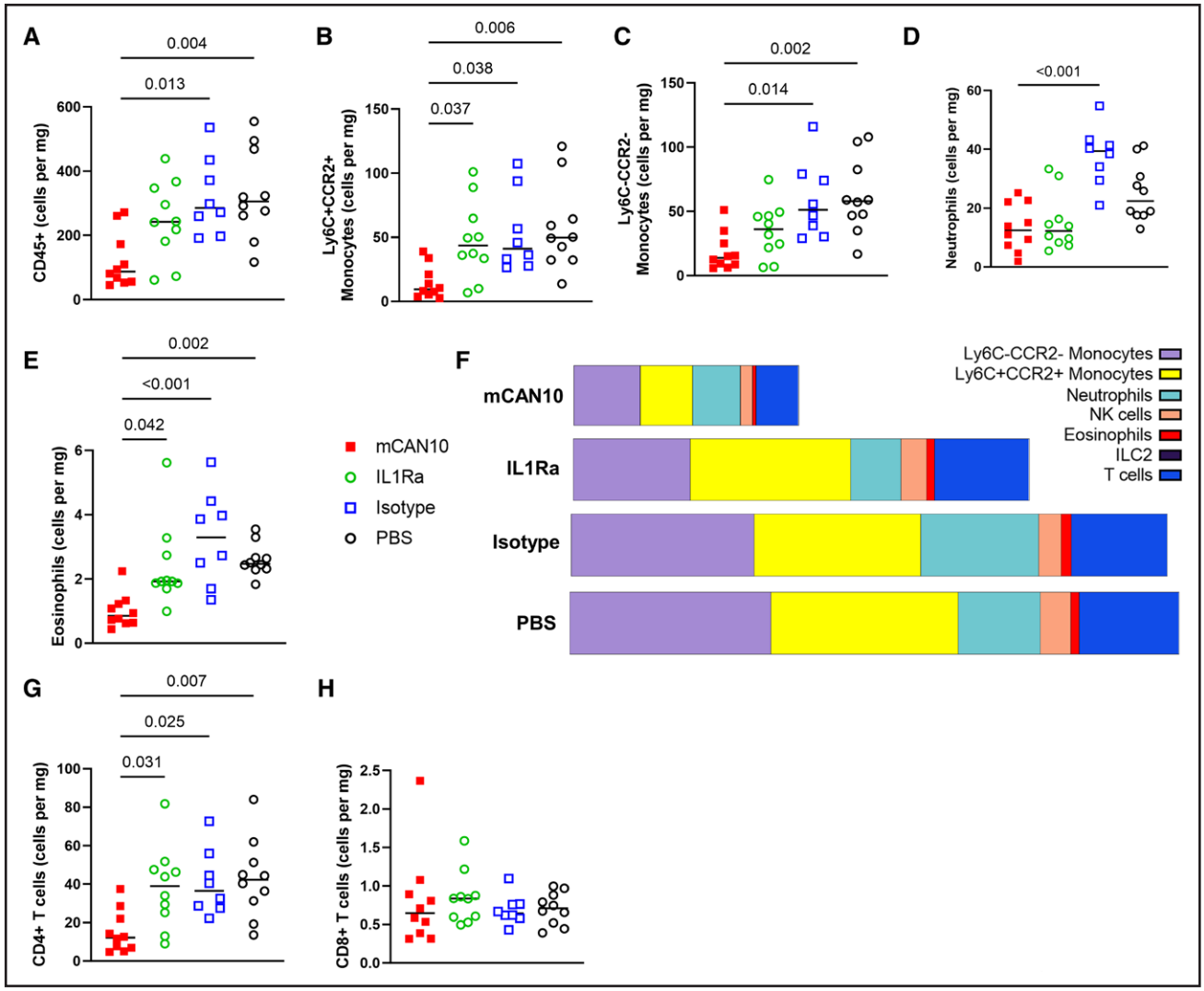

Figure 3. mCAN10 reduces cardiac immune populations during acute viral myocarditis.
A through **H**, Mice were infected with CVB3 and treated with mCAN10, isotype control, IL1Ra (interleukin-1 receptor antagonist), or PBS for 10 days. Flow cytometry was used to quantify immune populations in the heart, expressed as cell numbers per milligram of cardiac tissue (mCAN10, IL1Ra, and PBS, n=10; isotype, n=8). **F**, Average composition of immune cell populations for each treatment group. Bar size is proportional to cell number per milligram of the heart tissue. 1 cm^2=40 cells/mg. **A** through **H**, Data are representative of 2 independent experiments, only 1 of which is shown. **A** through **E**, **G**, and **H**, Kruskal-Wallis test with Dunn multiple pairwise comparisons. *P* values are presented only where the difference between the groups was significant. All other intergroup comparisons were nonsignificant. CVB3 indicates coxsackievirus B3; ILC2, innate lymphoid cells type 2; and NK, natural killer.

with viral myocarditis, and while it was enriched in the inflammatory foci, it was activated also in neighboring areas without histologically apparent immune population restriction (Figure 5B). mCAN10 treatment greatly reduced areas showing NFκB pathway gene expression, and these were primarily located to the immune foci themselves.

To further investigate the observed therapeutic effects of mCAN10 treatment, we used the SPADE analysis to identify spatially variable genes between mCAN10 and the isotype control. We further focused our analysis to compare immune foci ($CD45^+$ spots) and fibroblasts (*Pdgfra*$^+$ *Ptprc*$^-$ spots) separately and independently. Downstream signaling components of IL1RAP, such as *Irak2*, were downregulated in immune foci, while *MAP3k6* was downregulated in fibroblasts (Figure 5F). Additionally, the mCAN10 treatment impacted IFN-specific STAT expression, such as *Stat1* and *Stat2*, which was downregulated in the mCAN10-treated immune foci. *Stat4* was also downregulated in the fibroblasts of mCAN10-treated hearts (Figure 5F). Importantly, immune foci expressed less chemokine genes such as *Ccl6*, *Ccl8*, *Cxcl5*, and *Cxcl10*, while fibroblasts expressed less *Ccl5* and *Cxcl10* in mCAN10-treated hearts (Figure 5F). Finally, MHC-II antigen presentation genes such as *H2-Ab1* and *H2-Eb1* were downregulated in immune foci and fibroblasts in heart of mice treated with mCAN10 compared with their isotype counterparts (Figure 5F).

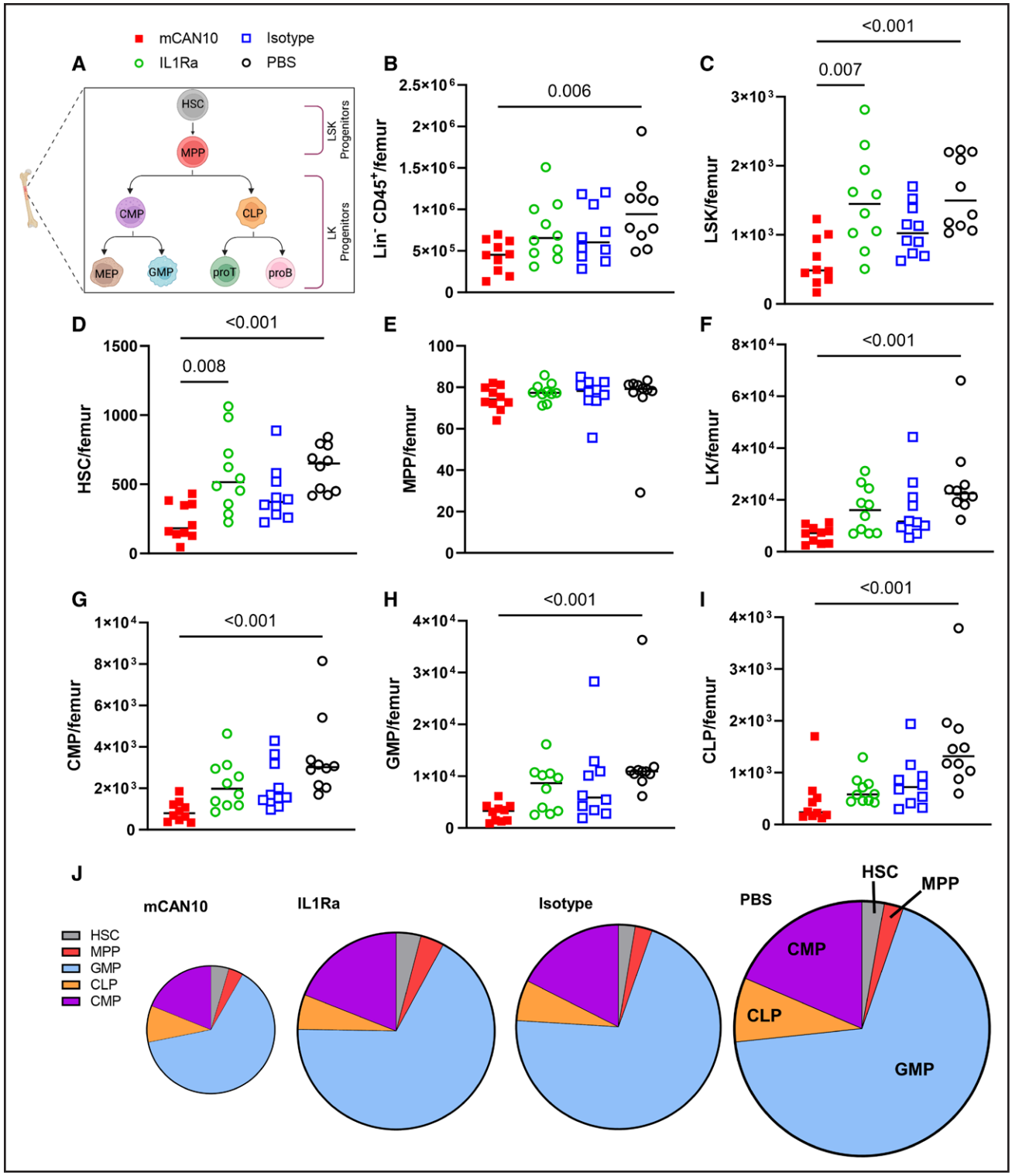

Figure 4. mCAN10 decreases inflammatory leukocyte precursors in the bone marrow during acute viral myocarditis.
Mice were infected with CVB3 and treated with mCAN10, isotype control, IL1Ra (interleukin-1 receptor antagonist), or PBS for 10 days (n=10 per group). **A**, Diagram of bone marrow progenitor population differentiation. **B** through **I**, Flow cytometry was used to quantify bone marrow precursor populations, expressed as cell numbers per femur, at day 10 post-infection. **J**, Average composition of bone marrow progenitor cell populations for each treatment group. Size is proportional to cell number per femur, 1 cm^2=6.01×10^4 cells/mg. Kruskal-Wallis test with Dunn multiple pairwise comparisons. *P* values are presented only where the difference between the groups was significant. All other intergroup comparisons were nonsignificant. CLP indicates common lymphoid progenitor; CMP, common myeloid progenitor; CVP3, coxsackievirus B3; GMP, granulocyte-monocyte precursor; HSC, hematopoietic stem cell; Lin, lineage; LK, $Lineage^{neg}Sca\text{-}1^{-}c\text{-}Kit^{+}$ precursor; LSK, $Lineage^{neg}Sca\text{-}1^{+}c\text{-}Kit^{+}$ precursor; MEP, megakaryocyte-erythrocyte precursor; and MPP, multipotent progenitor.

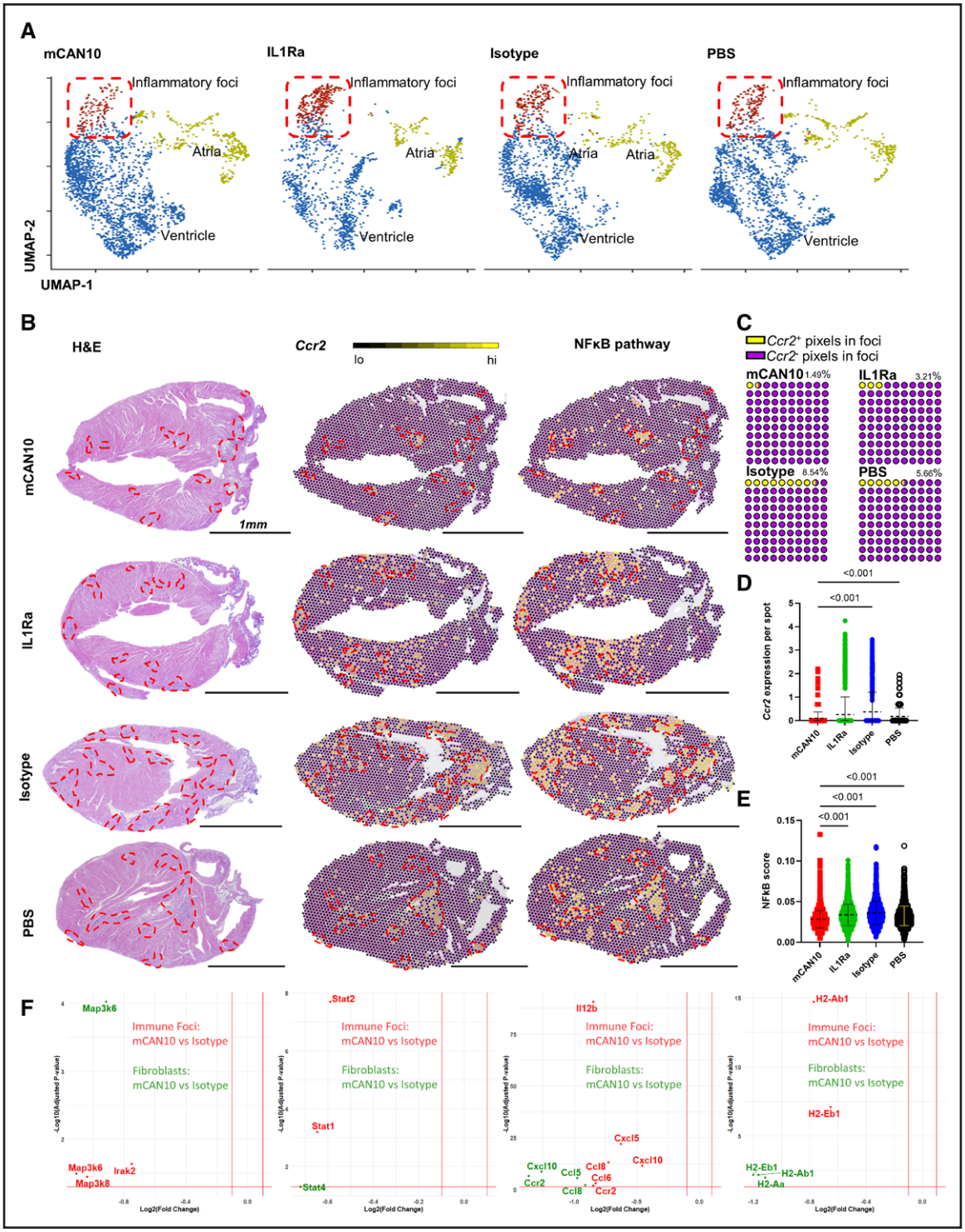

Figure 5. mCAN10 reduces inflammatory gene signaling in cardiac immune foci.

A, UMAP clustering of spatial transcriptomics gene sequencing spots of acute viral myocarditis heart slides from each treatment group (each group, n=1 slide). The dashed line indicates the cluster corresponding to manually annotated inflammatory foci spots. **B**, Visualization of expression of selected genes and pathways in cardiac tissue during acute viral myocarditis. Immune foci are recognized in H&E stains and circled in red dashed lines, which were overlaid on the spatial gene expression images. Scale bar=1 mm. **C** through **E**, Quantification of spatial gene expression data. **C**, Percentage of *Ccr2*-expressing pixels in the delineated immune foci. **D** and **E**, Quantification of gene or gene pathway expression levels. Data are represented as mean±SD. **F**, SPADE analysis was utilized to compare 10× Genomics Visium spatial transcriptomic data sets between H&E-stained slides from mCAN10-treated and isotype-treated mice on day 10 post-infection. The SPADE analysis focused on 4 molecular pathways: IL (interleukin)-1 downstream signaling, type 1 IFN (interferon) downstream signaling, proinflammatory response, and MHC-II antigen presentation. The plots show genes differentially downregulated in mCAN10-treated immune foci-specific spots or fibroblast-specific spots relative to their isotype-treated counterparts, stratified by the molecular pathway. Genes differentially expressed in (*Continued*)

We next investigated cell-cell communication. Communication through CCL chemokines demonstrated a communication direction toward inflammatory foci (Figure S4B), facilitating immune cell infiltration by chemokine receptor–expressing leukocytes (eg, CCR2$^+$ monocytes). We also visualized and quantified areas of T helper cell least (Th) 1, Th2, and Th17 response genes. mCAN10 treatment also reduced these responses, highlighting the broad anti-inflammatory properties of concomitant IL-1, IL-33, and IL-36 blockade (Figure S4C).

IL1RAP Blockade With mCAN10 Protects Against EAM

To investigate the therapeutic potential of mCAN10 in ameliorating long-term cardiac dysfunction in myocarditis, we used the experimental mouse model of chronic autoimmune myocarditis (EAM). We induced EAM in mice by immunization with the αMyHC peptide in complete Freund adjuvant on days 0 and 7. Treatment with mCAN10, anti-IL-1β antibody, or controls was initiated on day 7, at the time of the booster immunization (n=10 mice per group). Echocardiography was performed on days 0, 28, and 42 to analyze the effects of the treatments on long-term cardiac function (Figure 6A). Compared with the mouse IgG2a isotype control group, mCAN10-treated animals had preserved EF on day 28 (58.2% versus 52.7%; *P*=0.002) and day 42 (56.5% versus 51.0%; *P*=0.002; Figure 6B through 6D; Figure S5A). The anti-IL-1β treatment also led to improved EF compared with its isotype control (day 28: 54.7% versus 50.7%, *P*=0.021; day 42: 51.4% versus 48.2%, *P*=0.067; Figure 6B). The mCAN10-treated mice also had significantly higher EF compared with mice receiving anti-IL-1β treatment (day 28: 58.2% versus 54.7%, *P*=0.044; day 42: 56.5% versus 51.4%, *P*=0.003; Figure 6B). The left ventricular stroke volume and cardiac output were also best preserved in mice receiving anti-IL1RAP (Figure S5B and S5C). The heart rate did not differ among the different treatment groups across the duration of the experiment (Figure S5D). In subsequent experiments, we assessed whether treatment with IL1Ra or general immunosuppression by prednisone can reproduce the therapeutic effects of mCAN10. Neither treatment was able to improve long-term cardiac function in the EAM model (Figure S5E and S5F).

To characterize the effects of mCAN10 on the inflammatory infiltrate in the myocardium, we quantified the presence of macrophages and neutrophils on day 21 by immunohistochemistry (n=6–8 per group). We found fewer CD68$^+$ macrophages in the hearts of mCAN10-treated animals compared with isotype (*P*=0.056) or PBS (*P*=0.034; Figure 6E; Figure S5G). Ly6G$^+$ neutrophils were significantly lower in the mCAN10 group compared with the anti-IL-1β group on day 42 post-induction (*P*=0.013; Figure 6F; Figure S5H).

To study whether IL1RAP blockade maintains efficiency in already established myocarditis, we delayed the start of the treatments until day 14 (Figure 6G; n=10 mice per group). We assessed the inflammatory infiltrate by H&E and myocardial fibrosis by Masson trichrome staining on day 42. mCAN10 reduced myocarditis severity (1.0 versus 2.0 in isotype controls, *P*<0.001; and 1.7 in PBS-treated mice, *P*=0.014) and cardiac fibrosis (9.3% versus 12.3% in isotype controls, *P*=0.026; and 11.2% in PBS-treated mice, *P*=0.032; Figure 6H and 6I). The delayed mCAN10 treatment also prevented EF deterioration compared with the isotype controls and the PBS group (Figure 6J).

DISCUSSION

Myocarditis is an inflammatory disease of the heart that can lead to rapid degradation of cardiac function, in some cases necessitating circulatory support or heart transplantation.[34] Patients who develop cardiac dysfunction and fibrosis have a 50% 10-year survival rate.[35] Treatments are primarily supportive, with end-stage disease ultimately requiring heart transplant in the most severe cases. Immunosuppressive therapies have been used for treatment of giant-cell myocarditis and improved overall and transplant-free survival.[36] However, biological treatments that specifically address the immune cross-communication networks involved in the pathogenesis of myocarditis are missing. In this regard, cytokine-neutralizing antibodies have revolutionized the therapy of many inflammatory conditions.[37] The anti-IL-1β antibody canakinumab is a recent example of successful translation of this concept to cardiovascular pathology.[8] In myocarditis, several case reports have shown a beneficial effect of IL-1 inhibition using anakinra in severe forms of the disease.[38,39] The recently concluded ARAMIS trial (Androgen Receptor Antagonizing Agent for Metastasis-Free Survival) included patients with acute myocarditis treated with anakinra during hospitalization to reduce myocarditis complications.[40] The trial was neutral due to the low incidence of complications in the majority of the participants, underlying the importance of adequate selection of deteriorating patients in need of immunomodulation.

Figure 5 Continued. immune foci-specific spots are shown in red, and genes differentially expressed in fibroblast-specific spots are shown in green. *P* values are presented only where the difference between the groups was significant. All other intergroup comparisons were nonsignificant. H&E indicates hematoxylin and eosin; MCH-II, major histocompatibility complex class II; SPADE, Spatial Deconvolution for Domain Specific Cell-Type Estimation; and UMAP, uniform manifold approximation and projection.

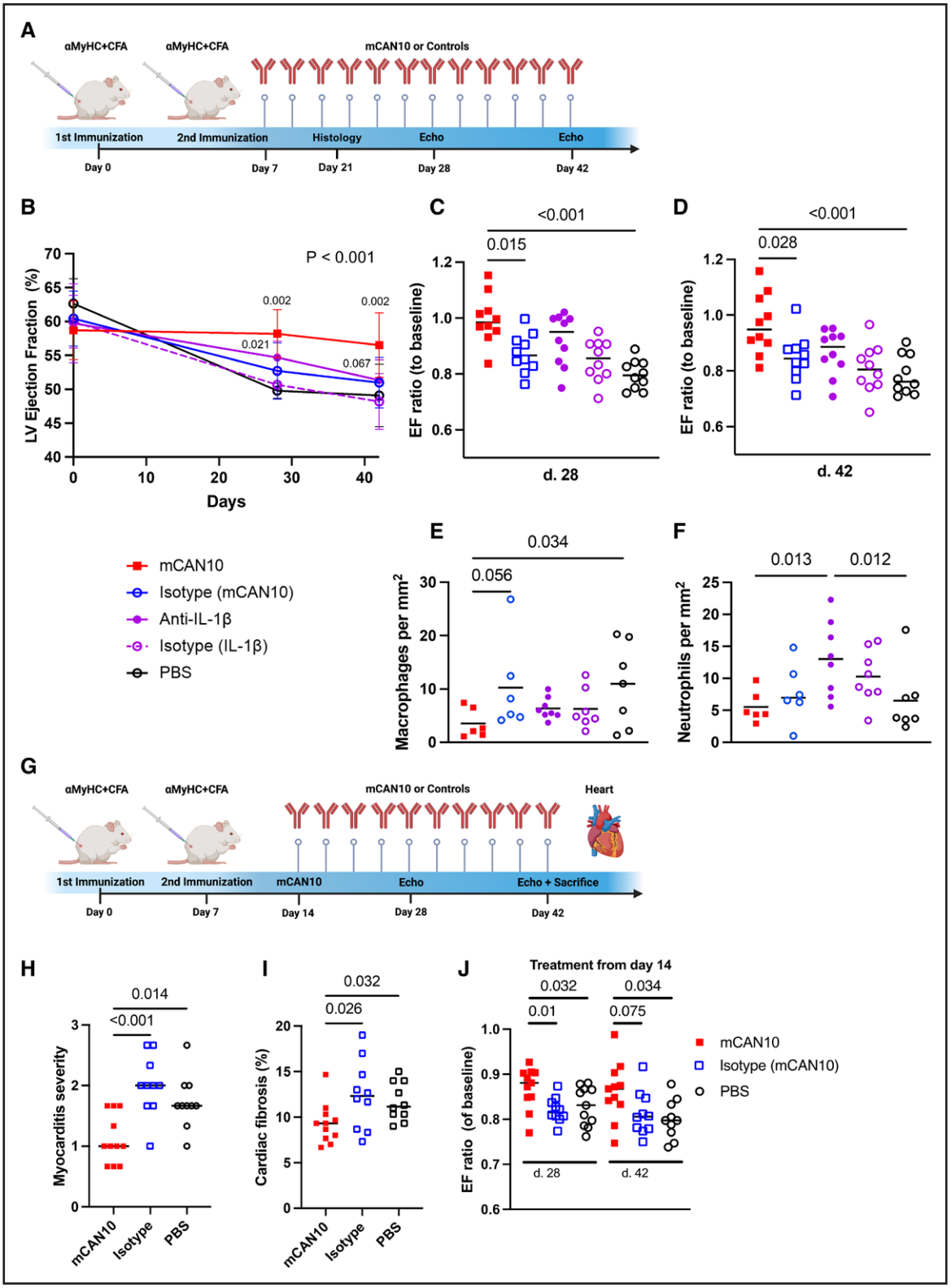

Figure 6. IL1RAP (interleukin-1 receptor accessory protein) blockade reduces the severity of experimental autoimmune myocarditis and preserves heart function.

A, EAM was induced by immunization with αMyHC (α-myosin heavy-chain peptide) in CFA on days 0 and 7. The mCAN10 and anti-IL (interleukin)-1β antibodies, their respective control isotypes, or PBS were administered intraperitoneally twice a week starting on day 7, at the time of the booster immunization (n=10 per group). **B**, Change in left ventricular EF from baseline to days 28 and 42 post-induction, 2-way repeated measures ANOVA (*P*<0.001). The *P* values above the data points refer to comparisons between the mCAN10 and anti-IL-1β treatment groups and their respective isotype controls by Fisher LSD post hoc test. Data are presented as (*Continued*)

We identified IL1RAP as a promising treatment target in myocarditis, with a central role in myocardial inflammation. We propose that IL1RAP blockade could be a good therapeutic approach to block IL-1 signaling in myocarditis, with additional anti-inflammatory effects provided by simultaneous neutralization of IL-33 and IL-36.[21] We found that blockade of IL1RAP by the mCAN10 antibody provided protection against viral and autoimmune myocarditis in mice. The treatment reduced myocardial inflammation and progression to fibrosis and significantly improved long-term cardiac function in the chronic EAM model.

In line with our hypothesis, IL1RAP neutralization affected the majority of the cardiac immune populations studied. In our CVB3 studies, IL1Ra treatment did not recapitulate the disease improvement that was seen in previously published preclinical studies of IL-1 signaling in CVB3 myocarditis.[19,20] This discrepancy may be due to the different methods of viral myocarditis induction, different animal strains used, and different methods of targeting IL-1 signaling. Treatment with anti-IL-1β antibodies was not as effective as mCAN10 in EAM, indicating that synergistic coblockade of IL-33 and IL-36 amplifies the immunomodulatory and anti-inflammatory effects. This hypothesis is supported by studies using MyD88 knockout mice. MyD88 is a downstream factor of several toll-like receptor pathways but also of the IL1RAP-dependent IL-1, IL-33, and IL-36 signaling cascades. In line with our data, genetic knockout of MyD88 resulted in protection against CVB3 viral myocarditis.[18]

There is additional evidence indicating that IL-33 and IL-36 blockade could contribute to the beneficial effects of IL1RAP blockade in myocarditis. The reduction of neutrophils with mCAN10 was likely aided by concomitant IL-36 blockade, a cytokine with an emerging role in neutrophilic infiltration in lung[41] and skin[42] inflammatory diseases, among others. A previous study found that neutralization of IL-38, a naturally occurring IL-36 antagonist, exacerbates CVB3 myocarditis,[15] indirectly indicating that IL-36 blocking contributes to disease amelioration by mCAN10. We and others have previously described the pathogenic role of IL-33 in inducing eosinophilic myopericarditis.[10,43] After ischemic or immune damage to the heart, Sca-1$^+$ inflammatory cardiac fibroblasts secrete IL-33, which activates cardiac resident ILC2s.[12] ILC2s, in turn, produce IL-5 and IL-13, which cause cardiac fibroblasts to secrete eotaxin that induces eosinophilic chemotaxis.[11,12,43] IL1RAP blockade reduced the infiltration of eosinophils into CVB3-infected hearts, likely by direct effects on eosinophils but potentially also by disrupting the fibroblast-ILC2 axis. IL-33 induces alternative macrophage activation by rewiring their cellular metabolism to uncouple the respiratory chain, which results in GATA3 (GATA binding protein 3) activation.[44] Alternatively activated macrophages aid in necrotic cell clearance, inflammation resolution, and tissue repair with protective effects in CVB3 myocarditis.[45] While mCAN10 blocks IL-33 signaling, it did not decrease mannose receptor CD206 expression in macrophages, a marker of alternative activation. This suggests that IL1RAP blockade did not affect macrophage polarization, perhaps due to concomitant blockade of other proinflammatory signals given via IL1RAP.

Cardiovascular insults augment myelopoiesis and granulopoiesis, and the resulting increase in systemic inflammatory leukocytes accelerates cardiovascular disease. IL-1β is one of the most important signals that accelerate these processes. IL-1β production in atherosclerotic plaques induces pathogenic leukocyte proliferation in the bone marrow, and IL-1β or NLRP3 (NOD-like receptor family pyrin domain containing 3) inflammasome inhibition dampens this phenomenon.[46] Myocardial infarction results in NLRP3 inflammasome activation of neutrophils in the heart, which reverse migrate to the bone marrow where they secrete local IL-1β, driving granulopoiesis.[46] mCAN10 reduced the number of cardiac neutrophils, possibly by similar IL-1β–blocking mechanisms.

Spatial transcriptomics has been previously validated to characterize inflammatory gene expression patterns in murine reovirus myocarditis[47,48] but not yet during CVB3 myocarditis. Our spatial gene expression studies revealed important reduction in the expression of canonical inflammatory genes and pathways with mCAN10 treatment. We were able to localize their expression to the characteristically patchy and disperse immune foci of acute viral myocarditis, enabling focused analysis in affected areas of the heart, as opposed to global analysis. One downfall of analyzing spatial transcriptomic data sets is the scarcity of analytical tools that compare spatially variable genes across spatial transcriptomic slides. However, the new SPADE analytical tool was recently released, enabling the comparative analysis of variable genes between 2 spatial

Figure 6 Continued. mean±SD. **C** and **D**, Comparison of EF ratio between groups at days 28 and 42 post-EAM induction, expressed as the proportion of baseline EF. **E**, Myocardial infiltration of CD68$^+$ (cluster of differentiation 68) macrophages on day 21. **F**, Myocardial infiltration of Ly6G$^+$ (lymphocyte antigen 6 complex, locus G) neutrophils on day 21. **G**, For the delayed treatment experiment, treatment was started on day 14 post-induction using the same treatment regimen as in **A** (mCAN10, n=11; isotype and PBS groups, n=10). **H**, Comparison of myocarditis severity score between treatment groups on day 42. **I**, Comparison of myocardial fibrosis among treatment groups on day 42, expressed as the percentage of left ventricular area. **J**, Comparison of EF ratio between groups, expressed as the proportion of baseline EF, on days 28 and 42 post-EAM induction. Data are presented as individual data points and median value for each group, except for **B**. Between-group comparisons were performed by the Kruskal-Wallis test with Dunn multiple comparisons post hoc test. *P* values are presented only where the difference between the groups was significant or where there was a clear trend. All other intergroup comparisons were nonsignificant. CD68 indicates cluster of differentiation 86; CFA, complete Freund adjuvant; EAM, experimental autoimmune myocarditis; EF, ejection fraction; LSD, least significant difference; and Ly6G, lymphocyte antigen 6 complex locus G6D.

transcriptomic slides.[49] Interestingly, mCAN10 led to a decline in expression of both IL-1 (*Irak2*) signaling and IFN signaling components (*Stat1* and *Stat2)* within immune foci. The decline in *Stat1* and *Stat2* expression may be a secondary consequence of the overall decline in inflammation or of blocking IL-33 signaling, which augments IFNγ production by effector T cells.[50–52] Furthermore, diminished *Stat1* signaling could contribute to the observed decline in MHC-II–expressing monocytes seen by flow cytometry and spatial transcriptomics, as *Stat1* signaling mediates IFNγ-induced upregulation of MHC-II expression.[53] Loss of local MHC-II expression on APCs and stromal cells could have contributed to the observed decline in CD4 responses.[54] Moreover, spatial gene expression analysis demonstrated that mCAN10 reduced expression of chemokines such as CCL5 (RANTES [regulated on activation normal T-cell expressed and secreted]), CCL8 (MCP-2), and CXCL10 (C-X-C motif chemokine ligand 10; IP10 [interferon-inducible protein 10]), suggesting that the decrease in monocyte, neutrophil, and T-cell infiltrations at least partially occurs through diminished chemokine activity.

In susceptible mice, acute EAM can progress to dilated cardiomyopathy. Our results demonstrated that mCAN10 protects EAM mice from cardiac dysfunction and even late administration provided treatment benefit. EAM mice develop dilated cardiomyopathy in an IL-17–dependent fashion involving cardiac remodeling, fibrosis, and loss of contractility.[55,56] $CCR2^+$ cardiac macrophages secrete IL-1β post-myocardial infarction, which activates familial adenomatous polyposis fibroblasts to induce collagen deposition, and these negative effects can be prevented by an anti-IL-1β antibody.[57] $Ly6C^+CCR2^+$ cardiac monocyte depletion protects from progression to dilated cardiomyopathy,[55] and their reduction with mCAN10 could contribute to the benefit of the treatment by reducing long-term fibrosis. Additionally, IL-1β induces IL-17 production by $CD4^+$ and γδ T cells.[58] IL1RAP blockade could disrupt the IL-1–IL-17 axis, which is known to promote autoimmunity and fibrosis.[59] A decrease in the Th17 transcriptional signature with mCAN10 treatment was observed in our spatial analysis, which may contribute to the cardioprotective properties of mCAN10.

We utilized 2 murine models of myocarditis, CVB3 myocarditis and EAM.[16] EAM is a Th17-driven murine model of autoimmune myocarditis, mostly resembling giant-cell myocarditis in humans. We have previously shown that IL-17A signaling to cardiac fibroblasts induces production of chemokines that drive the recruitment of neutrophils and inflammatory monocytes to the heart. This pathway is essential for the development of dilated cardiomyopathy and cardiac fibrosis.[55,56,60] Th17 cell induction is largely driven by the IL-1 pathway. In contrast, CVB3 myocarditis is Th1 driven. The IL-1 family serves as crucial signaling molecules in both the innate and adaptive immune systems, playing a pivotal role in promoting cardiac inflammation during myocarditis.[18–20] Upon activation of innate immune responses, cytokines such as IL-33, IL-1, and IL-36 are rapidly released, signaling to both hematopoietic and nonhematopoietic cells. The IL1RAP signaling stimulates the production of chemokines and cytokines and facilitates the recruitment of leukocytes to the heart, underscoring the important role of IL1RAP in innate immune response in myocarditis. However, later in the myocarditis timeline, as adaptive immune cells become predominant in cardiac inflammation, myeloid cells persist as a continuous source of IL-1β, IL-33, and IL-36. Moreover, IL-1 signaling extends to T cells, contributing to the polarization of Th17 cells. These Th17 cells produce profibrotic cytokines that drive cardiac remodeling and the progression of dilated cardiomyopathy, thus linking innate and adaptive immune responses in myocarditis. Despite the differences in the pathogenesis of EAM and CVB3 myocarditis, we have shown that IL1RAP signaling contributes to the pathogenesis of both these mice models and promote severe myocarditis.

Our study has a few limitations that should be considered. First, we used different mouse models to test treatment efficacy in acute and chronic myocarditis. The EAM model has been chosen for chronic myocarditis to avoid potential bias induced by the death of the sickest animals in the EVB3 model. As the acute EVB3 myocarditis experiments were terminated on day 10, we were not able to assess the potential long-term beneficial effects of delayed mCAN10 treatment in this model or whether mCAN10 would interfere with viral clearance. Second, as the spatial transcriptomics analysis has not been performed in EAM experiments, it remains to be determined whether similar pathways are affected by treatment in the acute phase of the disease as in the EVB3-infected mice. Finally, although the flow cytometry and spatial transcriptomics analyses have been performed in a standardized fashion, as described in Methods, we cannot completely exclude involuntary bias due to the identity of the groups being known to the observers. However, the validity of these analyses is supported by the results of the blinded histological, immunohistochemical, and functional analyses, which are in complete agreement. In addition, our study was completed only in males. Myocarditis is more prevalent in men compared with women, and the same bias is seen in animal models of myocarditis; therefore, male mice were used in this study.[61–63]

In conclusion, we show that the IL1RAP-blocking monoclonal antibody mCAN10 has a broad and potent anti-inflammatory profile in viral and autoimmune myocarditis, reducing myocardial inflammation and fibrosis and preserving cardiac function. A humanized anti-IL1RAP antibody (CAN10) blocking IL-1, IL-33, and IL-36 signaling without eliciting FcR-mediated effector functions is currently undergoing testing in a phase 1 clinical trial on healthy subjects and subjects with plaque psoriasis (NCT06143371). This antibody holds promise as a potential future treatment for patients with severe myocarditis.

ARTICLE INFORMATION

Received February 21, 2024; accepted September 24, 2024.

Affiliations

Department of Pathology, School of Medicine (D.A.L., D.E., M.V.T., D.Č.), W. Harry Feinstone Department of Molecular Microbiology and Immunology, Bloomberg School of Public Health (A.D., H.K., D.Č.), and Department of Cardiology, School of Medicine (N.W.), Johns Hopkins University, Baltimore, MD. Department of Translational Medicine, Lund University, Malmö, Sweden (G.J., A.S.). Cantargia AB, Lund, Sweden (S.R., C.G., E.J.G., D.L.). Internal Medicine Clinic, Skåne University Hospital, Lund, Sweden (A.S.). "Nicolae Simionescu" Institute of Cellular Biology and Pathology, Bucharest, Romania (A.S.).

Acknowledgments

The authors acknowledge the Johns Hopkins University (JHU) Ross Flow Cytometry Core for use of their instruments, specifically Cytek Aurora (funded by National Institutes of Health grant S10OD026859). They also acknowledge the JHU Single Cell and Transcriptomics Core for facilitating the spatial transcriptomics experiments. Figures 2A, 4A, 6A, and 6E were created with BioRender.com. Conceptualization: Drs Schiopu and Čiháková; methodology: Drs Rattik, Lema, Grönberg, and Jaensson Gyllenbäck; formal analysis: Dr Lema, G. Jakobsson, A. Daoud, Dr Elias, Dr Grönberg, Dr Jaensson Gyllenbäck, and Dr Rattik; investigation: Dr Lema, G. Jakobsson, M.V. Talor, Dr Kalinoski, and N. Wang; resources: Drs Rattik, Lema, and Grönberg; writing—original draft: Dr Lema; writing—review and editing: Dr Elias, Dr Rattik, Dr Liberg, Dr Grönberg, Dr Jaensson Gyllenbäck, G. Jakobsson, Dr Schiopu, and Dr Čiháková; visualization: Dr Lema, A. Daoud, Dr Rattik, and Dr Grönberg; supervision: Drs Schiopu and Čiháková; and project administration: Drs Schiopu and Čiháková.

Sources of Funding

This study was funded by project-specific funding from Cantargia AB.

Disclosures

Drs Rattik, Grönberg, Jaensson Gyllenbäck, and Liberg are employees of Cantargia AB; are on patents related to anti-IL1RAP (interleukin-1 receptor accessory protein) monoclonal antibodies owned by Cantargia AB; and have stocks or stock options as employees of Cantargia AB. The other authors report no conflicts.

Supplemental Material

Figures S1–S5

REFERENCES

1. Fung G, Luo H, Qiu Y, Yang D, McManus B. Myocarditis. *Circ Res*. 2016;118:496–514. doi: 10.1016/S0140-6736(11)60648-X
2. Bowles NE, Ni J, Kearney DL, Pauschinger M, Schultheiss HP, McCarthy R, Hare J, Bricker JT, Bowles KR, Towbin JA. Detection of viruses in myocardial tissues by polymerase chain reaction. Evidence of adenovirus as a common cause of myocarditis in children and adults. *J Am Coll Cardiol*. 2003;42:466–472. doi: 10.1016/s0735-1097(03)00648-x
3. Kandolin R, Lehtonen J, Salmenkivi K, Räisänen-Sokolowski A, Lommi J, Kupari M. Diagnosis, treatment, and outcome of giant-cell myocarditis in the era of combined immunosuppression. *Circ Heart Fail*. 2013;6:15–22. doi: 10.1161/CIRCHEARTFAILURE.112.969261
4. Pollack A, Kontorovich AR, Fuster V, Dec GW. Viral myocarditis--diagnosis, treatment options, and current controversies. *Nat Rev Cardiol*. 2015;12:670–680. doi: 10.1038/nrcardio.2015.108
5. Swindell WR, Beamer MA, Sarkar MK, Loftus S, Fullmer J, Xing X, Ward NL, Tsoi LC, Kahlenberg MJ, Liang Y, et al. RNA-Seq analysis of IL-1B and IL-36 responses in epidermal keratinocytes identifies a shared MyD88-dependent gene signature. *Front Immunol*. 2018;9:80. doi: 10.3389/fimmu.2018.00080
6. Højen JF, Kristensen MLV, McKee AS, Wade MT, Azam T, Lunding LP, de Graaf DM, Swartzwelter BJ, Wegmann M, Tolstrup M, et al. IL-1R3 blockade broadly attenuates the functions of six members of the IL-1 family, revealing their contribution to models of disease. *Nat Immunol*. 2019;20:1138–1149. doi: 10.1038/s41590-019-0467-1
7. Ridker PM, Everett BM, Thuren T, MacFadyen JG, Chang WH, Ballantyne C, Fonseca F, Nicolau J, Koenig W, Anker SD, et al; CANTOS Trial Group. Antiinflammatory therapy with canakinumab for atherosclerotic disease. *N Engl J Med*. 2017;377:1119–1131. doi: 10.1056/NEJMoa1707914
8. Ridker PM, MacFadyen JG, Everett BM, Libby P, Thuren T, Glynn RJ; CANTOS Trial Group. Relationship of C-reactive protein reduction to cardiovascular event reduction following treatment with canakinumab: a secondary analysis from the CANTOS randomised controlled trial. *Lancet*. 2018;391:319–328. doi: 10.1016/S0140-6736(17)32814-3
9. Ghali R, Altara R, Louch WE, Cataliotti A, Mallat Z, Kaplan A, Zouein FA, Booz GW, Booz GW. IL-33 (interleukin 33)/sST2 axis in hypertension and heart failure. *Hypertension*. 2018;72:818–828. doi: 10.1161/HYPERTENSIONAHA.118.11157
10. Abston ED, Barin JG, Cihakova D, Bucek A, Coronado MJ, Brandt JE, Bedja D, Kim JB, Georgakopoulos D, Gabrielson KL, Fairweather D, et al. IL-33 independently induces eosinophilic pericarditis and cardiac dilation: ST2 improves cardiac function. *Circ Heart Fail*. 2012;5:366–375. doi: 10.1161/CIRCHEARTFAILURE.111.963769
11. Choi HS, Won T, Hou X, Chen G, Bracamonte-Baran W, Talor MV, Jurčová I, Szárszoi O, Čurnova L, Stříž I, et al. Innate lymphoid cells play a pathogenic role in pericarditis. *Cell Rep*. 2020;30:2989–3003.e6. doi: 10.1016/j.celrep.2020.02.040
12. Bracamonte-Baran W, Chen G, Hou X, Talor MV, Choi HS, Davogustto G, Taegtmeyer H, Sung J, Hackam DJ, Nauen D, et al. Non-cytotoxic cardiac innate lymphoid cells are a resident and quiescent type 2-commited population. *Front Immunol*. 2019;10:634. doi: 10.3389/fimmu.2019.00634
13. El-Awaisi J, Kavanagh DP, Rink MR, Weston CJ, Drury NE, Kalia N. Targeting IL-36 improves age-related coronary microcirculatory dysfunction and attenuates myocardial ischemia/reperfusion injury in mice. *JCI Insight*. 2022;7:e155236. doi: 10.1172/jci.insight.155236
14. Luo C, Xie X, Feng X, Lei B, Fang C, Li Y, Cai X, Ling G, Zheng B. Deficiency of interleukin-36 receptor protected cardiomyocytes from ischemia-reperfusion injury in cardiopulmonary bypass. *Med Sci Monit*. 2020;26:e918933–e918933. doi: 10.12659/MSM.918933
15. Xue Y, Chen M, Chen Q, Huang T, Fan Q, Lin F, Ke J, Chen F. Neutralization of interleukin-38 exacerbates coxsackievirus B3-induced acute myocarditis in mice. *Virol J*. 2021;18:220. doi: 10.1186/s12985-021-01687-w
16. Čiháková D, Rose NR. Myocarditis and other immunological models of cardiac disease. In: Ardehali H, ed. *Manual of Research Techniques in Cardiovascular Medicine*. John Wiley and Sons Ltd; 2014:197–202.
17. Tschöpe C, Ammirati E, Bozkurt B, Caforio ALP, Cooper LT, Felix SB, Hare JM, Heidecker B, Heymans S, Hübner N, et al. Myocarditis and inflammatory cardiomyopathy: current evidence and future directions. *Nat Rev Cardiol*. 2021;18:169–193. doi: 10.1038/s41569-020-00435-x
18. Fuse K, Chan G, Liu Y, Gudgeon P, Husain M, Chen M, Yeh WC, Akira S, Liu PP. Myeloid differentiation factor-88 plays a crucial role in the pathogenesis of coxsackievirus B3-induced myocarditis and influences type I interferon production. *Circulation*. 2005;112:2276–2285. doi: 10.1161/CIRCULATIONAHA.105.536433
19. Kraft L, Erdenesukh T, Sauter M, Tschope C, Klingel K. Blocking the IL-1beta signalling pathway prevents chronic viral myocarditis and cardiac remodeling. *Basic Res Cardiol*. 2019;114:11. doi: 10.1007/s00395-019-0719-0
20. Lim BK, Choe SC, Shin JO, Ho SH, Kim JM, Yu SS, Kim S, Jeon ES. Local expression of interleukin-1 receptor antagonist by plasmid DNA improves mortality and decreases myocardial inflammation in experimental coxsackieviral myocarditis. *Circulation*. 2002;105:1278–1281.
21. Fields JK, Kihn K, Birkedal GS, Klontz EH, Sjöström K, Günther S, Beadenkopf R, Forsberg G, Liberg D, Snyder GA, et al. Molecular basis of selective cytokine signaling inhibition by antibodies targeting a shared receptor. *Front Immunol*. 2021;12:779100. doi: 10.3389/fimmu.2021.779100
22. Fontes JA, Barin JG, Talor MV, Stickel N, Schaub J, Rose NR, Cihakova D. Complete Freund's adjuvant induces experimental autoimmune myocarditis by enhancing IL-6 production during initiation of the immune response. *Immun Inflamm Dis*. 2017;5:163–176. doi: 10.1002/iid3.155
23. Kaplanov I, Carmi Y, Kornetsky R, Shemesh A, Shurin GV, Shurin MR, Dinarello CA, Voronov E, Apte RN. Blocking IL-1beta reverses the immunosuppression in mouse breast cancer and synergizes with anti-PD-1 for tumor abrogation. *Proc Natl Acad Sci USA*. 2019;116:1361–1369. doi: 10.1073/pnas.1812266115
24. Goncalves NP, Vieira P, Saraiva MJ. Interleukin-1 signaling pathway as a therapeutic target in transthyretin amyloidosis. *Amyloid*. 2014;21:175–184. doi: 10.3109/13506129.2014.927759
25. Li H, Zhang YY, Huang XY, Sun YN, Jia YF, Li D. Beneficial effect of tripterine on systemic lupus erythematosus induced by active chromatin in BALB/c mice. *Eur J Pharmacol*. 2005;512:231–237. doi: 10.1016/j.ejphar.2005.02.030
26. Diny NL, Baldeviano GC, Talor MV, Barin JG, Ong S, Bedja D, Hays AG, Gilotra NA, Coppens I, Rose NR, et al. Eosinophil-derived IL-4

drives progression of myocarditis to inflammatory dilated cardiomyopathy. *J Exp Med*. 2017;214:943–957. doi: 10.1084/jem.20161702
27. Lindsey ML, Kassiri Z, Virag JAI, de Castro Brás LE, Scherrer-Crosbie M. Guidelines for measuring cardiac physiology in mice. *Am J Physiol Heart Circ Physiol*. 2018;314:H733–h752. doi: 10.1152/ajpheart.00339.2017
28. Lasrado N, Borcherding N, Arumugam R, Starr TK, Reddy J. Dissecting the cellular landscape and transcriptome network in viral myocarditis by single-cell RNA sequencing. *iScience*. 2022;25:103865. doi: 10.1016/j.isci.2022.103865
29. Litviňuková M, Talavera-López C, Maatz H, Reichart D, Worth CL, Lindberg EL, Kanda M, Polanski K, Heinig M, Lee M, et al. Cells of the adult human heart. *Nature*. 2020;588:466–472. doi: 10.1038/s41586-020-2797-4
30. Velten L, Haas SF, Raffel S, Blaszkiewicz S, Islam S, Hennig BP, Hirche C, Lutz C, Buss EC, Nowak D, et al. Human haematopoietic stem cell lineage commitment is a continuous process. *Nat Cell Biol*. 2017;19:271–281. doi: 10.1038/ncb3493
31. Saunders KO. Conceptual approaches to modulating antibody effector functions and circulation half-life. *Front Immunol*. 2019;10:1296. doi: 10.3389/fimmu.2019.01296
32. Fairweather D, Rose NR. Coxsackievirus-induced myocarditis in mice: a model of autoimmune disease for studying immunotoxicity. *Methods*. 2007;41:118–122. doi: 10.1016/j.ymeth.2006.07.009
33. Hettwer J, Hinterdobler J, Miritsch B, Deutsch MA, Li X, Mauersberger C, Moggio A, Braster Q, Gram H, Robertson AAB, et al. Interleukin-1beta suppression dampens inflammatory leucocyte production and uptake in atherosclerosis. *Cardiovasc Res*. 2022;118:2778–2791. doi: 10.1093/cvr/cvab337
34. ElAmm CA, Al-Kindi SG, Oliveira GH. Characteristics and outcomes of patients with myocarditis listed for heart transplantation. *Circ Heart Fail*. 2016;9:e003259. doi: 10.1161/CIRCHEARTFAILURE.116.003259
35. Greulich S, Seitz A, Muller KAL, Grun S, Ong P, Ebadi N, Kreisselmeier KP, Seizer P, Bekeredjian R, Zwadlo C, et al. Predictors of mortality in patients with biopsy-proven viral myocarditis: 10-year outcome data. *J Am Heart Assoc*. 2020;9:e015351. doi: 10.1161/JAHA.119.015351
36. Bang V, Ganatra S, Shah SP, Dani SS, Neilan TG, Thavendiranathan P, Resnic FS, Piemonte TC, Barac A, Patel R, et al. Management of patients with giant cell myocarditis: JACC review topic of the week. *J Am Coll Cardiol*. 2021;77:1122–1134. doi: 10.1016/j.jacc.2020.11.074
37. Caforio AL, Pankuweit S, Arbustini E, Basso C, Gimeno-Blanes J, Felix SB, Fu M, Helio T, Heymans S, Jahns R, et al; European Society of Cardiology Working Group on M and Pericardial D. Current state of knowledge on aetiology, diagnosis, management, and therapy of myocarditis: a position statement of the European Society of Cardiology working group on myocardial and pericardial diseases. *Eur Heart J*. 2013;34:2636–48, 2648a–2648d. doi: 10.1093/eurheartj/eht210
38. Cavalli G, Pappalardo F, Mangieri A, Dinarello CA, Dagna L, Tresoldi M. Treating life-threatening myocarditis by blocking interleukin-1. *Crit Care Med*. 2016;44:e751–e754. doi: 10.1097/CCM.0000000000001654
39. Parisi F, Paglionico A, Varriano V, Ferraccioli G, Gremese E. Refractory adult-onset Still disease complicated by macrophage activation syndrome and acute myocarditis: a case report treated with high doses (8 mg/kg/d) of anakinra. *Medicine (Baltim)*. 2017;96:e6656. doi: 10.1097/MD.0000000000006656
40. Morrow DA, Verbrugge FH. In-perspective: the ARAMIS double-blind randomized placebo-controlled trial of anakinra for the treatment of acute myocarditis. *Eur Heart J Acute Cardiovasc Care*. 2023;12:627–628. doi: 10.1093/ehjacc/zuad102
41. Koss CK, Wohnhaas CT, Baker JR, Tilp C, Przibilla M, Lerner C, Frey S, Keck M, Williams CMM, Peter DEl Kasmi KC, et al. IL36 is a critical upstream amplifier of neutrophilic lung inflammation in mice. *Commun Biol*. 2021;4:172. doi: 10.1038/s42003-021-01703-3
42. Todorović V, Su Z, Putman CB, Kakavas SJ, Salte KM, McDonald HA, Wetter JB, Paulsboe SE, Sun Q, Gerstein CE, et al. Small molecule IL-36γ antagonist as a novel therapeutic approach for plaque psoriasis. *Sci Rep*. 2019;9:9089. doi: 10.1038/s41598-019-45626-w
43. Diny NL, Hou X, Barin JG, Chen G, Talor MV, Schaub J, Russell SD, Klingel K, Rose NR, Cihakova D. Macrophages and cardiac fibroblasts are the main producers of eotaxins and regulate eosinophil trafficking to the heart. *Eur J Immunol*. 2016;46:2749–2760. doi: 10.1002/eji.201646557
44. Faas M, Ipseiz N, Ackermann J, Culemann S, Gruneboom A, Schroder F, Rothe T, Scholtysek C, Eberhardt M, Bottcher MKronke G, et al. IL-33-induced metabolic reprogramming controls the differentiation of alternatively activated macrophages and the resolution of inflammation. *Immunity*. 2021;54:2531–2546 e5. doi: 10.1016/j.immuni.2021.09.010
45. Wang C, Dong C, Xiong S. IL-33 enhances macrophage M2 polarization and protects mice from CVB3-induced viral myocarditis. *J Mol Cell Cardiol*. 2017;103:22–30. doi: 10.1016/j.yjmcc.2016.12.010
46. Sreejit G, Nooti SK, Jaggers RM, Athmanathan B, Park KH, Al-Sharea A, Johnson J, Dahdah A, Lee MKS, Ma J, et al. Retention of the NLRP3 inflammasome–primed neutrophils in the bone marrow is essential for myocardial infarction–induced granulopoiesis. *Circulation*. 2022;145:31–44. doi: 10.1161/CIRCULATIONAHA.121.056019
47. Mantri M, Hinchman MM, McKellar DW, Wang MFZ, Cross ST, Parker JSL, De Vlaminck I. Spatiotemporal transcriptomics reveals pathogenesis of viral myocarditis. *Nat Cardiovasc Res*. 2022;1:946–960. doi: 10.1038/s44161-022-00138-1
48. McKellar DW, Mantri M, Hinchman MM, Parker JSL, Sethupathy P, Cosgrove BD, De Vlaminck I. Spatial mapping of the total transcriptome by in situ polyadenylation. *Nat Biotechnol*. 2023;41:513–520. doi: 10.1038/s41587-022-01517-6
49. Lu Y, Chen QM, An L. SPADE: Spatial Deconvolution for Domain Specific Cell-Type Estimation. *Commun Biol*. 2024;7:469. doi: 10.1038/s42003-024-06172-y
50. Komai-Koma M, Wang E, Kurowska-Stolarska M, Li D, McSharry C, Xu D. Interleukin-33 promoting Th1 lymphocyte differentiation dependents on IL-12. *Immunobiology*. 2016;221:412–417. doi: 10.1016/j.imbio.2015.11.013
51. Reichenbach DK, Schwarze V, Matta BM, Tkachev V, Lieberknecht E, Liu Q, Koehn BH, Pfeifer D, Taylor PA, Prinz G, et al. The IL-33/ST2 axis augments effector T-cell responses during acute GVHD. *Blood*. 2015;125:3183–3192. doi: 10.1182/blood-2014-10-606830
52. Yang Q, Li G, Zhu Y, Liu L, Chen E, Turnquist H, Zhang X, Finn OJ, Chen X, Lu B. IL-33 synergizes with TCR and IL-12 signaling to promote the effector function of CD8+ T cells. *Eur J Immunol*. 2011;41:3351–3360. doi: 10.1002/eji.201141629
53. Reith W, LeibundGut-Landmann S, Waldburger JM. Regulation of MHC class II gene expression by the class II transactivator. *Nat Rev Immunol*. 2005;5:793–806. doi: 10.1038/nri1708
54. Ngwenyama N, Kaur K, Bugg D, Theall B, Aronovitz M, Berland R, Panagiotidou S, Genco C, Perrin MA, Davis J, et al. Antigen presentation by cardiac fibroblasts promotes cardiac dysfunction. *Nat Cardiovasc Res*. 2022;1:761–774. doi: 10.1038/s44161-022-00116-7
55. Wu L, Ong S, Talor MV, Barin JG, Baldeviano GC, Kass DA, Bedja D, Zhang H, Sheikh A, Margolick JB, et al. Cardiac fibroblasts mediate IL-17A-driven inflammatory dilated cardiomyopathy. *J Exp Med*. 2014;211:1449–1464. doi: 10.1084/jem.20132126
56. Baldeviano GC, Barin JG, Talor MV, Srinivasan S, Bedja D, Zheng D, Gabrielson K, Iwakura Y, Rose NR, Cihakova D. Interleukin-17A is dispensable for myocarditis but essential for the progression to dilated cardiomyopathy. *Circ Res*. 2010;106:1646–1655. doi: 10.1161/CIRCRESAHA.109.213157
57. Amrute JM, Luo X, Penna V, Bredemeyer A, Yamawaki T, Yang S, Kadyrov F, Heo GS, Shi SY, Lee P, et al. Targeting immune-fibroblast cross-talk in myocardial infarction and cardiac fibrosis. *Res Sq*. 2023. doi: 10.21203/rs.3.rs-2402606/v1
58. Lalor SJ, Dungan LS, Sutton CE, Basdeo SA, Fletcher JM, Mills KHG. Caspase-1–processed cytokines IL-1β and IL-18 Promote IL-17 production by γδ and CD4 T cells that mediate autoimmunity. *J Immunol*. 2011;186:5738–5748. doi: 10.4049/jimmunol.1003597
59. Park MJ, Moon SJ, Lee EJ, Jung KA, Kim EK, Kim DS, Lee JH, Kwok SK, Min JK, Park SH, et al. IL-1-IL-17 signaling axis contributes to fibrosis and inflammation in two different murine models of systemic sclerosis. *Front Immunol*. 2018;9:1611. doi: 10.3389/fimmu.2018.01611
60. Hou X, Chen G, Bracamonte-Baran W, Choi HS, Diny NL, Sung J, Hughes D, Won T, Wood MK, Talor MV, et al. The cardiac microenvironment instructs divergent monocyte fates and functions in myocarditis. *Cell Rep*. 2019;28:172–189.e7. doi: 10.1016/j.celrep.2019.06.007
61. McNamara DM, Starling RC, Cooper LT, Boehmer JP, Mather PJ, Janosko KM, Gorcsan J 3rd, Kip KE, Dec GW; IMAC Investigators. Clinical and demographic predictors of outcomes in recent onset dilated cardiomyopathy: results of the IMAC (Intervention in Myocarditis and Acute Cardiomyopathy)-2 study. *J Am Coll Cardiol*. 2011;58:1112–1118. doi: 10.1016/j.jacc.2011.05.033
62. Onyimba JA, Coronado MJ, Garton AE, Kim JB, Bucek A, Bedja D, Gabrielson KL, Guilarte TR, Fairweather D. The innate immune response to coxsackievirus B3 predicts progression to cardiovascular disease and heart failure in male mice. *Biol Sex Differ*. 2011;2:2. doi: 10.1186/2042-6410-2-2
63. Cooper LT Jr. Myocarditis. *N Engl J Med*. 2009;360:1526–1538. doi: 10.1056/NEJMra0800028